November 1998 • NREL/SR-520-25844

Microstructure of Amorphous-Silicon-Based Solar Cell Materials by Small-Angle X-Ray Scattering

Final Subcontract Report 6 April 1994 - 30 June 1998

D.L. Williamson
Department of Physics
Colorado School of Mines
Golden, Colorado

National Renewable Energy Laboratory
1617 Cole Boulevard
Golden, Colorado 80401-3393
A national laboratory of the U.S. Department of Energy
Managed by Midwest Research Institute
for the U.S. Department of Energy
under contract No. DE-AC36-83CH10093

NREL/SR-520-25844

Microstructure of Amorphous-Silicon-Based Solar Cell Materials by Small-Angle X-Ray Scattering

Final Subcontract Report
6 April 1994 - 30 June 1998

D.L. Williamson
Department of Physics
Colorado School of Mines
Golden, Colorado

NREL technical monitor: B. von Roedern

National Renewable Energy Laboratory
1617 Cole Boulevard
Golden, Colorado 80401-3393
A national laboratory of the U.S. Department of Energy
Managed by Midwest Research Institute
for the U.S. Department of Energy
under contract No. DE-AC36-83CH10093

Prepared under Subcontract No. XAN-4-13318-04

November 1998

This publication was reproduced from the best available copy
Submitted by the subcontractor and received no editorial review at NREL

NOTICE

This report was prepared as an account of work sponsored by an agency of the United States government. Neither the United States government nor any agency thereof, nor any of their employees, makes any warranty, express or implied, or assumes any legal liability or responsibility for the accuracy, completeness, or usefulness of any information, apparatus, product, or process disclosed, or represents that its use would not infringe privately owned rights. Reference herein to any specific commercial product, process, or service by trade name, trademark, manufacturer, or otherwise does not necessarily constitute or imply its endorsement, recommendation, or favoring by the United States government or any agency thereof. The views and opinions of authors expressed herein do not necessarily state or reflect those of the United States government or any agency thereof.

Available to DOE and DOE contractors from:
Office of Scientific and Technical Information (OSTI)
P.O. Box 62
Oak Ridge, TN 37831
Prices available by calling (423) 576-8401

Available to the public from:
National Technical Information Service (NTIS)
U.S. Department of Commerce
5285 Port Royal Road
Springfield, VA 22161
(703) 605-6000 or (800) 553-6847
or
DOE Information Bridge
http://www.doe.gov/bridge/home.html

Printed on paper containing at least 50% wastepaper, including 10% postconsumer waste

1. EXECUTIVE SUMMARY

1.1 PREFACE

This report presents results of research performed from April 6, 1994 to June 30, 1998 under a cost-reimbursible subcontract from the National Renewable Energy Laboratory (NREL, a national laboratory of the U.S. Department of Energy operated by Midwest Research Institute) to the Colorado School of Mines (subcontract number XAN-4-13318-04 to the prime contract DE-AC02-83CH10093). The research was carried out under the direction of Don L. Williamson, Professor of Physics. Materials characterization, including small-angle x-ray scattering, x-ray diffraction, and flotation density, were carried out in the Physics Department of the Colorado School of Mines. The materials for analyses were supplied by NREL-supported device-making groups as well as by other groups with relevant expertise. Electron microprobe analyses of film compositions were carried out by Alice Mason of NREL. TEM measurements were made by Kim Jones of NREL. Graduate students Donghoon Min, Troy Berens, Steve Johnston, and Nam Hyun Kang contributed to the research project.

1.2 OBJECTIVES/APPROACH

The general objective of this research was to provide detailed microstructural information on the amorphous-silicon-based, thin-film materials under development for improved multijunction solar cells. Correlation of this microstructure with opto-electronic properties and device performance was an integral part of the research. The principal experimental technique used was small-angle x-ray scattering (SAXS) and it provided quantitative microstructural data on microvoid fractions, sizes, shapes, and their preferred orientations. Other microstructural features such as alloy segregation, hydrogen-rich clusters and alloy short-range order were probed. In the later stages of the project, considerable effort was devoted to characterization of medium range order and microcrystallinity using conventional wide-angle x-ray diffraction. In addition, access was obtained to anomalous SAXS facilities in Germany for measurements on the Ge uniformity in a-SiGe:H alloys. Three types of material were investigated and these matched the bandgap classification scheme forming the basis of three of the four NREL Amorphous Silicon Teams. Specific conclusions from a wide variety of experiments are presented below separated into the low-gap, mid-gap, and high-gap materials.

1.3 CONCLUSIONS

1.3.1 Low-Gap Materials

Hydrogen dilution - H_2 dilution during deposition of a-$Si_{1-x}Ge_x$:H alloys does not lead to unique microstructure modifications. Some conditions produce improvements in homogeneity while others lead to more highly oriented microstructure.

Ion bombardment - Deposition conditions that generate more ion bombardment of the a-$Si_{1-x}Ge_x$:H film surface during growth yield significantly improved microstructures, often leading to undetectable levels of nanovoids (≤0.01 vol.%).

Microwave deposition - High-deposition-rate a-$Si_{1-x}Ge_x$:H alloys made by a microwave PECVD method are highly inhomogeneous unless a high dc bias is applied to the substrate during deposition. This bias induces ion bombardment and nearly homogeneous material.

Helium dilution - a-Si:H produced by He dilution yields highly homogeneous material with optical gaps as low as 1.50 eV. Attempts to produce solar cells of this material by USSC with reduced V_{oc} were not successful.

Hotwire deposition - The first a-$Si_{1-x}Ge_x$:H alloys made by the hotwire method showed non-homogeneous microstructures similar to those prepared by PECVD. The transition to the structurally inferior state occurred at lower x than found for PECVD alloys.

Ge uniformity - Several a-$Si_{1-x}Ge_x$:H alloys show clear evidence of inhomogeneous Ge distributions as determined by ASAXS. This nonuniformity is removed by enhanced ion bombardment during growth and it is reduced by hydrogen dilution of the plasma.

Record solar cell material - The bottom and middle layers of the world record 13.0% stabilized efficiency device made by USSC show significantly inhomogeneous microstructures with clear orientational features.

Thermal stability - Several a-$Si_{1-x}Ge_x$:H alloys show microstructural changes induced by annealing at 300°C and above. Nanovoids form in higher H content samples and one sample showed improvements in microstructure upon annealing.

1.3.2 Mid-Gap Materials

Absolute intensity and device-quality a-Si:H - The SAXS data were placed on an absolute intensity scale and the lower detection limit of microvoids was found to be around 0.01 vol.% in a-Si:H for the SAXS facility and typical a-Si:H film thicknesses provided (1 to 3 μm). Typical behavior of the best device quality PECVD material was found to be near or below this detection limit.

Staebler-Wronski effect - Comparison of precision, in-situ SAXS results for 4 a-Si:H samples in the light-soaked (1000 h at 1 Sun) state and the annealed state reveal no detectable differences in SAXS-determined microstructure.

Model a-Si and a-Si:H - Void-free a-Si and a-Si:H could be produced by implantation techniques. Lack of voids allowed the conclusion that the well-defined density deficit of 1.8% in a-Si compared to c-Si must be due to an average bond length increase in the amorphous state. A solubility limit of 3 to 4 at.% H was found for a-Si:H produced by implantation of H. Concentrations higher than this lead to nanobubble formation upon annealing above 300°C.

Similar behavior is found for PECVD a-Si:H but the solubility limit is higher.

Device-quality hotwire material - The hotwire material developed at NREL for devices has less than 0.01 vol.% nanovoids, similar to the best PECVD material. The hotwire a-Si:H has much less H and a flotation density of 2.29 g/cm^3, only 1.8% less than c-Si, compared to values of 2.20 to 2.25 g/cm^3 for PECVD material. Small increases in the amount of microstructure are induced by annealing device-quality hotwire material at only 250°C, well below the deposition temperature of 375°C.

Ar dilution - The microstructure of a-Si:H can be affected by Ar dilution of the silane plasma. There is a minimum in the amount of heterogeneity near 90% Ar dilution and this shows a strong correlation with a minimum in the Urbach energy and the defect density.

Boron doping - Doping of PECVD a-Si:H via 1% TMB in He leads to dramatic increases in the nanovoid density, and a correlation with subsequent photoluminescence intensity of anodically etched porous films.

Medium-range order and microcrystallinity - Conventional wide-angle x-ray diffraction provides evidence through a narrowing of the first peak in the x-ray pattern that the medium-range order of hotwire a-Si:H is improved with increasing substrate temperature. This may be related to the improved light stability of the hotwire material. Further narrowing of the first x-ray peak is observed for films that are partially microcrystalline. Microcrystallinity can be detected and studied in films as thin as 0.4 μm.

Record solar cell material - The a-Si:H material used in the top cell of the USSC triple-junction, world record device (13.0% stabilized efficiency) has an undetectable nanovoid fraction (≤0.01 vol.%) but a clear signal due to larger-scale inhomogeneity. This behavior is similar to all device-quality a-Si:H films that yield the best solar cells.

1.3.3 High-Gap Materials

Microvoid density in a-SiC:H - All a-$Si_{1-x}C_x$:H alloys examined show a similar result of high densities (1-2 vol.%) of spherical-like nanovoids only about 1 nm in diameter. There is always a broad maximum or shoulder in the SAXS data indicating an interparticle interference effect that is never seen in a-Si:H or a-SiGe:H.

ECD high V_{oc} material - A film of a-Si:H prepared by ECD with the same conditions used for the i-layer of a high V_{oc} cell (1.04 V initial) shows no detectable nanovoids and a flotation density consistent with about 18 at.% H.

TIT chemical annealing material - Films of a-Si:H prepared by the "chemical annealing" method at the Tokyo Institute of Technology (I. Shimizu et al) have high H contents (up to 24 at.%) and high optical gaps (up to 2.05 eV). Such films have considerable microstructure with void contents up to 1.2 vol.%, about 2 orders of magnitude larger that device-quality PECVD

and hotwire material.

IACS hotwire-assisted PECVD material - Films of a-$Si_{1-x}C_x$:H prepared by a hybrid hotwire/PECVD method to try to combine the advantages of both show the typical microstructure of C-containing alloys, 1-nm-sized voids at the 1 vol.% level. IACS finds evidence of improved light stability for this material.

Thermal Stability of a-SiC:H - Nanovoid fractions increase systematically in several a-$Si_{1-x}C_x$:H alloys upon annealing above 300°C suggesting H-diffusion-controlled growth and clustering of H in nanovoids.

Table of Contents

1. Executive Summary---------- 3
  1.1 Preface---------- 3
  1.2 Objectives/Approach---------- 3
  1.3 Conclusions---------- 3

Table of Contents---------- 7
List of Figures---------- 8
List of Tables---------- 9

2. Introduction---------- 10
3. Results and Discussion---------- 11
  3.1 Low-Gap Materials---------- 11
  3.2 Mid-Gap Materials---------- 31
  3.3 High-Gap Materials---------- 36
4. References---------- 47

List of Figures

Fig. 1. SAXS intensities from the USSC microwave-deposited a-$Si_{1-x}Ge_x$:H alloys---------- 13
Fig. 2. SAXS intensities from IACS He-diluted a-Si:H films------------------------------------ 16
Fig. 3. Effect of tilting of sample on SAXS intensity of an IACS He-diluted film-------------- 16
Fig. 4. SAXS from USSC films prepared to represent the three intrinsic layer of the recent triple-junction, world record efficiency device--- 18
Fig. 5. More direct comparison of SAXS from top layer (a-Si:H) and bottom layer (a-$Si_{0.5}Ge_{0.5}$:H) by normalizing to the same electron density and diffuse intensity------------ 18
Fig. 6. SAXS from hotwire a-$Si_{1-x}Ge_x$:H alloy (x=0)--- 21
Fig. 7. SAXS from hotwire a-$Si_{1-x}Ge_x$:H alloy (x=0.13)-- 22
Fig. 8. SAXS from hotwire a-$Si_{1-x}Ge_x$:H alloys (x=0.19 and 0.23)------------------------------ 23
Fig. 9. Composition dependence of integrated SAXS intensities from hotwire a-$Si_{1-x}Ge_x$:H alloys and USSC PECVD a-$Si_{1-x}Ge_x$:H alloys------------------------------------- 25
Fig. 10. SAXS data from annealing study of Harvard a-$Si_{1-x}Ge_x$:H sample--------------------- 28
Fig. 11. SAXS data from annealing study of USSC a-$Si_{1-x}Ge_x$:H sample----------------------- 28
Fig. 12. SAXS data from annealing study of USSC a-$Si_{1-x}Ge_x$:H sample----------------------- 29
Fig. 13. Overview of annealing study results from USSC and Harvard samples----------------- 30
Fig. 14. Diffuse SAXS intensities versus annealing--- 30
Fig. 15. Average diameter of scattering features from SAXS data versus annealing----------- 31
Fig. 16. SAXS data comparing states A and B via in-situ annealing method-------------------- 32
Fig. 17. Effect of annealing on the nanostructure of hotwire a-Si:H------------------------------ 35
Fig. 18. SAXS from ECD a-Si:H, high V_{oc} material--- 37
Fig. 19. Standard x-ray diffraction data from TIT series #1 films--------------------------------- 39
Fig. 20. SAXS from TIT series #1 a-Si:H films and from NREL device-quality film---------- 41
Fig. 21. SAXS data from TIT series #2 films-- 43
Fig. 22. Effect of tilting on SAXS from one of the TIT series #2 films--------------------------- 43
Fig. 23. SAXS data from IACS a-$Si_{1-x}C_x$:H alloys--- 44
Fig. 24. Variation of the integrated SAXS intensities (Q) from a-SiC:H films versus anneal temperature and time--- 46
Fig. 25. Typical SAXS data from the Iowa State a-SiC:H alloys and the interference model fits--- 47

List of Tables

Table 1. SAXS results from series of five microwave-deposited a-$Si_{1-x}Ge_x$:H alloys--------- 12

Table 2. Results for IACS Series of He-diluted a-Si:H films-- 15

Table 3. SAXS results from USSC triple-junction solar cell i-layers------------------------------ 17

Table 4. Hotwire a-$Si_{1-x}Ge_x$:H alloys prepared for SAXS study------------------------------------ 19

Table 5. SAXS results for hotwire a-$Si_{1-x}Ge_x$:H alloys-- 24

Table 6. Results of SAXS tilting experiments for several hotwire a-$Si_{1-x}Ge_x$:H alloys--------- 26

Table 7. Alloys selected for thermal stability study-- 27

Table 8. a-Si:H films selected for the Staebler-Wronski effect study------------------------------ 32

Table 9. Deposition conditions and properties of TIT high optical gap a-Si:H films------------ 39

Table 10. Flotation density results for TIT series #1 samples-- 40

Table 11. SAXS results from TIT series # 1 samples--- 41

Table 12. SAXS and flotation density results from TIT series # 2 samples---------------------- 43

Table 13. Composition, SAXS, and flotation density results for IACS a-$Si_{1-x}C_x$:H------------ 45

2. INTRODUCTION

A wide array of experiments have been completed during the last four years in collaboration with NREL, NREL-supported groups, and other groups with expertise in amorphous silicon related materials and devices. The results and discussion of these experiments will be broken into sections according to whether the materials are low-gap, mid-gap, and high-gap, consistent with the NREL team structure. Since many of the experiments have been described in detail in publications, these will be given a brief summary and the reader interested in more details can refer to the relevant publications. For those experiments not yet described in publications, detailed results and discussions will be provided in this report.

In the area of low-gap materials, the following experiments were carried out. The microstructural effects of deposition parameters (H_2 dilution, ion bombardment) and new techniques (microwave and hotwire deposition) were investigated in the preparation of a-$Si_{1-x}Ge_x$:H. Preparation of lower gap a-Si:H by He dilution was examined. Thermal stability of a selected set of these alloys was also examined via annealing experiments. A new small-angle technique, anomalous SAXS (ASAXS), was used for the first time to investigate the uniformity of Ge in several a-$Si_{1-x}Ge_x$:H alloys. The a-$Si_{1-x}Ge_x$:H material used in the latest world-record efficiency a-Si-based solar cell (USSC) was examined.

Several experiments were done with mid-gap materials. Calibrations were made in order to place the SAXS data on an absolute intensity scale (electron units) such that void fractions could be calculated independent of the secondary calibration used earlier based on flotation density. A systematic light-soaking experiment was performed with four a-Si:H films to look for any structural differences in the A and B states. Model samples of a-Si and a-Si:H were made by ion implantation to study by SAXS, IR, SIMS, and TEM. Results from such samples were compared to those from conventional PECVD material. SAXS measurements were made on low-H-content hotwire a-Si:H material that was being used by NREL for the hotwire device development. An annealing experiment was performed on one of the hotwire samples to examine its stability. A series of samples prepared by IACS with Ar-dilution was examined. The effect of B doping on the microstructure was studied. Conventional wide-angle x-ray diffraction measurements were used to search for changes in medium range order and microcrystallinity in a wide variety of samples prepared by NREL. The top cell i-layer material of the world-record efficiency device made by USSC was characterized by SAXS.

A few high-gap materials were studied. After establishment of the absolute SAXS intensity scale, several a-SiC:H alloys were re-examined to determine their void fractions. One high-H-content film from ECD was prepared under similar conditions that gave their V_{oc}=1.04 V. A series of high-H-content films from TIT (Shimizu) prepared by the "chemical annealing" method was investigated. IACS prepared a series of a-SiC:H alloys by a new technique for SAXS

analysis. A systematic study was carried out of the effects of annealing on the microstructure of a-SiC:H alloys prepared by sputtering at Iowa State (Shinar).

3. RESULTS AND DISCUSSION

3.1 LOW-GAP MATERIALS

3.1.1 Hydrogen Dilution

The microstructure of two sets of a-$Si_{1-x}Ge_x$:H alloys prepared by PECVD, with and without hydrogen dilution of the source gases (silane and germane), have been analyzed by SAXS, IR spectroscopy, and flotation density measurements [1]. Optoelectronic properties of codeposited films have also been characterized [1]. Hydrogen dilution suppresses dihydride/polyhydride formation, reduces bonded H content, and reduces the SAXS-detected microstructure for $x>0$. Studies of anisotropy in the SAXS intensity indicate an increased amount of oriented microstructure as Ge is added, consistent with a trend toward columnarlike growth in both undiluted and hydrogen-diluted films, but the diluted films have a significantly reduced degree of such oriented microstructure. The improvement in the microstructure due to hydrogen dilution correlated with improvement of the optoelectronic properties. The modification of microstructure due to H_2 dilution of the source gases has been discussed in terms of growth mechanisms of alloy films. See reference 1 for all the details of this study.

In contrast, alloys made by USSC at "high" dilution showed a dramatic increase in oriented features. The latter features can be modeled by ellipsoidal objects that are 7 nm in average diameter and more than 20 times as long [2]. Based on quantitative analysis of the SAXS, we conclude that these highly elongated objects are low in density (0.6 vol.% if voids) and their strong preferred orientation parallel to the carrier conduction direction minimizes their effect on the device properties [2].

3.1.2 Ion Bombardment

Two experiments were done that involved explicit use of enhanced ion bombardment during deposition, deposition on the powered electrode of a PECVD system (Harvard) and application of a high substrate bias during microwave PECVD deposition (USSC). In the Harvard collaboration [3], films of a-$Si_{1-x}Ge_x$:H were deposited which possess optoelectronic properties that are greatly improved over any yet reported in the range $x \geq 0.6$. These films were deposited on the cathode (cathodic deposition) of an rf discharge. This allows for high levels of ion bombardment, and the deposition parameters are those that result in high electron temperature in the discharge plasma which is thought to lead to favorable chemical radicals. The film properties were assessed using a large variety of measurements and by comparison to the properties of alloys conventionally prepared on the anode (anodic deposition). Significant improvements are found in the photoconductivity and the ambipolar diffusion lengths. It was confirmed that the

improvements in phototransport are not due to a shift in the Fermi level. The improvements are attributed in large part to the reduction of long range structural heterogeneity observed by SAXS and electron microscopy, and partly to reduction of midgap state density. In spite of their superior properties, an assessment of the data of the cathodic alloys suggests that alloying introduces mechanisms detrimental to transport which are not present in a-Si:H or a-Ge:H. The Urbach tail width is 42±2 meV for cathodic a-Ge:H and 45±2 meV for cathodic a-$Si_{1-x}Ge_x$:H and is constant with x. From differences in band edges and tails it was inferred that the atomic bond ordering is different between anodic and cathodic alloys. A photoluminescence peak is observed with an intensity roughly an order of magnitude greater than for anodic alloys, and a significantly different peak energy. See reference 3 for all the details of this study.

Enhanced ion bombardment was used in a new technique involving microwave PECVD developed by USSC and this clearly led to improved microstructures. This study is described in detail in the next section.

3.1.3 Microwave Deposition

A series of five a-$Si_{1-x}Ge_x$:H alloys was deposited by a microwave plasma technique at USSC with high deposition rates from 1 to 4 nm/s and under different substrate bias conditions [4,5]. Table 1 and Figure 1 present the results of the SAXS analyses. Ge content and flotation densities are included in the table.

Table 1. SAXS results from series of five microwave-deposited a-$Si_{1-x}Ge_x$:H alloys.

sample # (prep. cond.)	x	ρ(flot) (g/cm^3)	ρ(crys) (g/cm^3)	t (μm)	Q_N (a)	I_d (e/a)	A (b)	<R> (nm)	$(Q_o/Q_{45})_N$	f_c (%)
2092 (4nm/s, low bias)	0.59	3.89	4.19	3.3	38	64	6	1.6	2.4	4.2
2093 (4nm/s, high bias)	0.54	3.99	4.04	2.2	<0.03	71	8	--	--	<0.01
2193 (2nm/s, high bias)	0.56	3.93	4.10	2.0	27	67	17	1.4	5.2	2.0
2303 (1nm/s, high bias)	0.62	>4.05	4.28	1.4	<0.03	105	22	--	--	<0.01
2304 (1nm/s, low bias)	0.65	4.05	4.36	1.3	58	61	23	1.6	2.9	5.3

a. Units = 10^{24}eu/cm^3; b. Units = eu/nm^3

Notes: x was determined at NREL by EPMA (Alice Mason); t is the thickness based on x-ray absorption; The subscript N indicates the Q's due only to the nanostructural features without the A/q^3 term [2]; f_c is the corrected void volume fraction based on the Q_o/Q_{45} ratio and the ellipsoidal model [2].

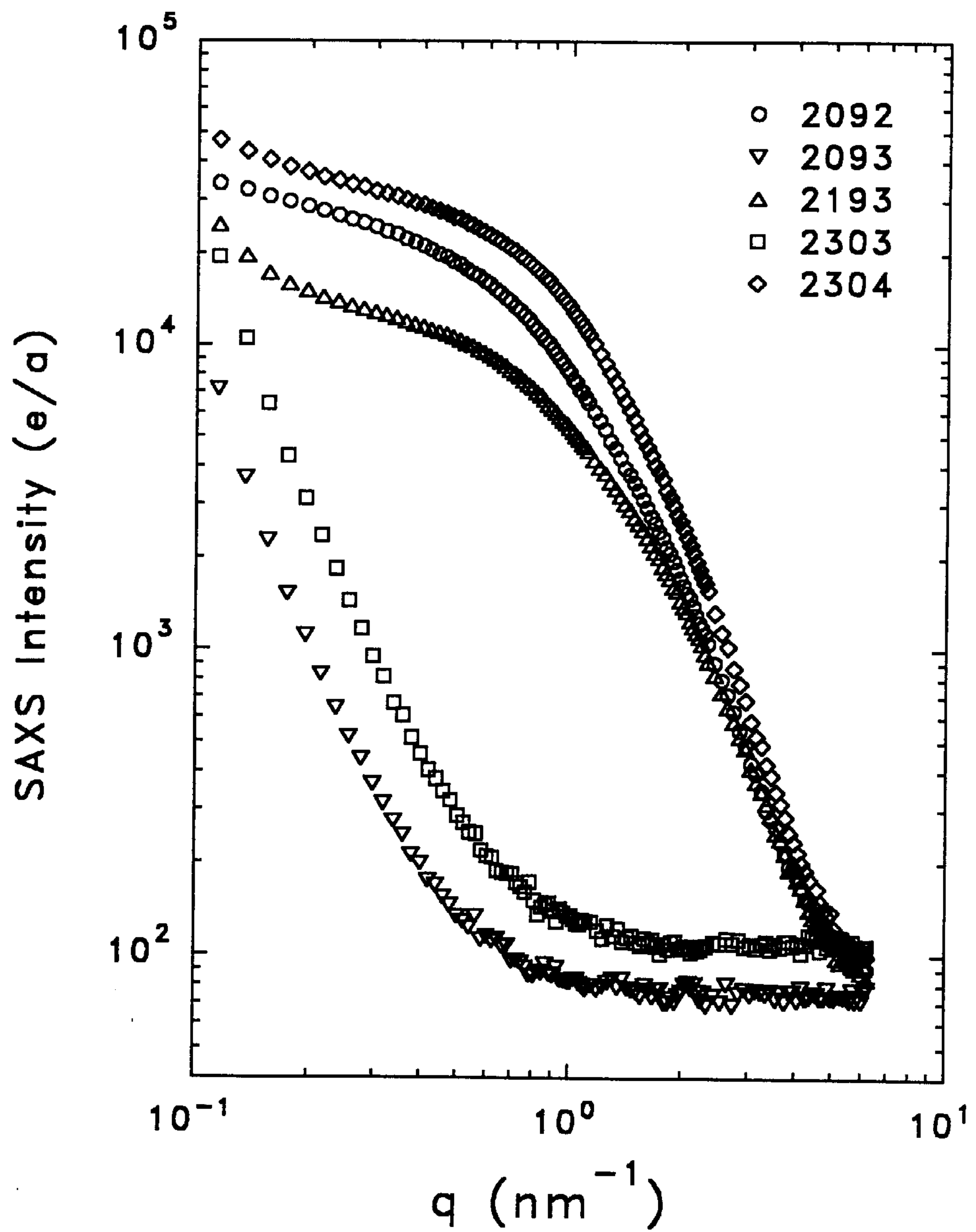

Fig. 1. SAXS intensities from the USSC microwave-deposited $a\text{-}Si_{1-x}Ge_x:H$ alloys.

Standard x-ray diffraction from all 5 samples shows no evidence of any crystallinity. The SAXS data in Fig. 1 and Table 1 show dramatic differences among the samples: 2093 and 2303 show no detectable Q_N, while 2093, 2193, and 2304 show very strong intensities and large Q_N. A noteworthy result is that 2193 does not seem to fit the trend of low SAXS when the bias is high during deposition. Solar cells made with high bias yield the best characteristics [5].

The x values and the flotation densities are nicely consistent. Table 1 includes the densities expected for crystalline alloys. Note that 4.05 g/cm^3 is the highest density we can measure due the limit of our fluid. The estimated void fractions (f_c) are all lower than the density deficits, $1 - \rho(\mathrm{flot})/\rho(\mathrm{crys})$, and this is readily explained by the H alloying effect (and perhaps an average bond-length increase in the amorphous state).

According to the EPMA analyses, samples 2092 and 2304 had quite significant oxygen contamination (4.7 and 14.1 at.%, resp.), consistent with the more porous nanostructure. The other samples were: 2093-1.1%, 2193-2.3%, 2303-2.2%. These oxygen contents were not included in the x values (i.e., x was based only on the Si/Ge ratios).

For the two samples with the very weak SAXS (2093, 2303), accurate values for the diffuse intensity, I_d, shows a higher level for 2303. This implies significantly more H in this sample.

The average radii, <R>, are quite small and represent the dimension obtained with the samples untilted. No values could be obtained for two samples due to undetectable Q_N's and the steep rise at low q for these two samples must be due to larger-scale features (R >10 nm) due either to surface roughness or some residual (weak) microstructure. The A's do show some tilt dependence such that $A_0/A_{45} = \sim 4$ for 2093 and ~10 for 2303.

More information has been obtained on some of these samples by ASAXS as presented later.

3.1.4 Helium Dilution

The a-Si group at IACS has developed a technique for fabricating lower bandgap a-Si:H using He dilution during high-pressure PECVD [6]. A series of 5 a-Si:H films prepared with 94% He dilution of a silane plasma and chamber pressures ranging from 0.5 to 2.0 Torr have been analyzed. The properties of the 5 films, the flotation densities, and the SAXS results are summarized in Table 2.

Figure 2 shows the SAXS data from all five samples. The SAXS intensity is very weak above q =1 nm^{-1} and is essentially independent of q in this range, corresponding to only diffuse scattering, I_d. There are steep rises at low q as characterized by the A parameter (coef. of q^{-3} term), indicating different amounts of some larger-scale microstructure (>20 nm). This

Table 2. Results for IACS Series of He-diluted a-Si:H films.

sample	E_{opt}(Tauc) (eV)	σ(dark) (S/cm)	ημτ (cm^2/V)	ρ(flot) (g/cm^3)	Q_N (eu/cm^3)	A (eu/nm^3)	I_d (eu)
P0	1.675	4.69E-10	1.91E-5	2.234	≤ 2E22	13.5[a]	16
P1	1.59	5.22E-10	1.84E-5	2.240	≤ 2E22	3.5	15
P3	1.54	3.33E-9	9.74E-5	2.226	≤ 2E22	2.5	15
P4	1.50	4.76E-9	5.57E-5	2.231	≤ 2E22	2.0[b]	14
P5	1.60	4.35E-9	2.90E-5	2.219	≤ 2E22	0.7	15

a. $A(0^o)/A(45^o) = 13.5/2$
b. $A(0^o)/A(45^o) = 2.0/0.2$

larger-scale structure has some orientation since Fig. 3 shows a tilting effect such that A decreases significantly upon tilting to 45 degrees. We are not able to detect any nanostructural SAXS (I_N) so that the integrated intensity due to such features (Q_N) is estimated to be less than $2x10^{22}$ eu/cm^3. The latter value corresponds to 0.01 vol.% nanovoids. Thus this He-diluted, low-gap material is quite homogeneous on this scale but contains a small amount of larger-scale features that seem to be related to residual columnar-like microstructure (in view of the tilting effect). The latter seems to decrease systematically with the number of the series (from P0 to P5).

Note that the flotation density is nearly constant at 2.23±0.01 g/cm^3 for all samples, consistent with no differences in nanovoid fractions among the samples. The density deficit compared to c-Si (2.33 g/cm^3) must be due to the H alloying and the likely bond-length extension in the amorphous state. We also checked all of the samples by conventional x-ray diffraction and found no evidence of microcrystallinity.

USSC made an attempt to reproduce this low-gap material in a device [7] but could not achieve a reduced V_{oc} that would have been consistent with such a lowering of the optical gap indicated in Table 2 (and Ref. 6). USSC noted that the detailed deposition geometry and conditions may be the origin of the differences [7].

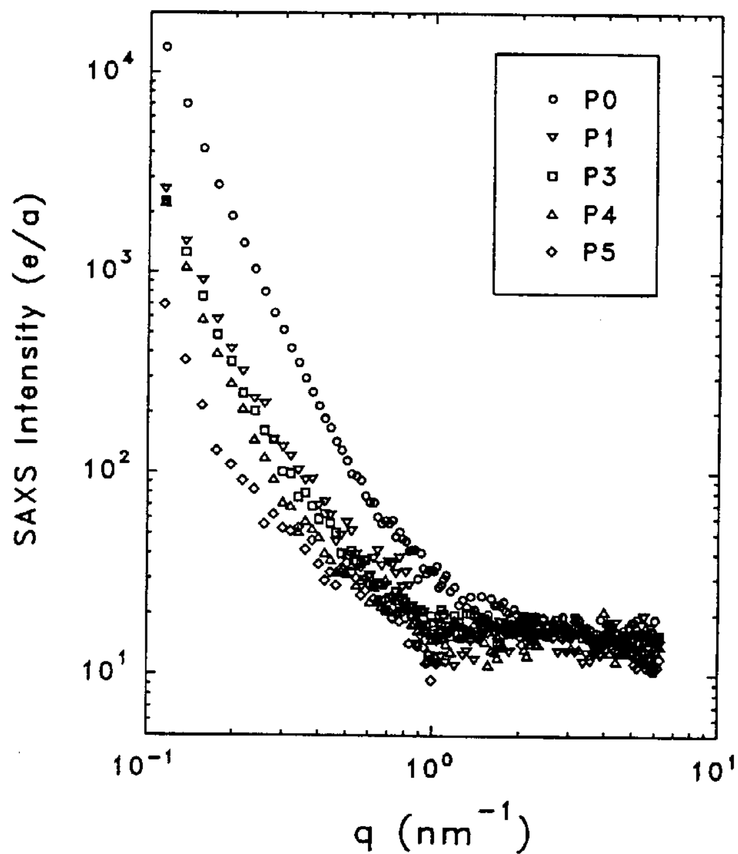

Fig .2. SAXS intensities from IACS He-diluted a-Si:H films.

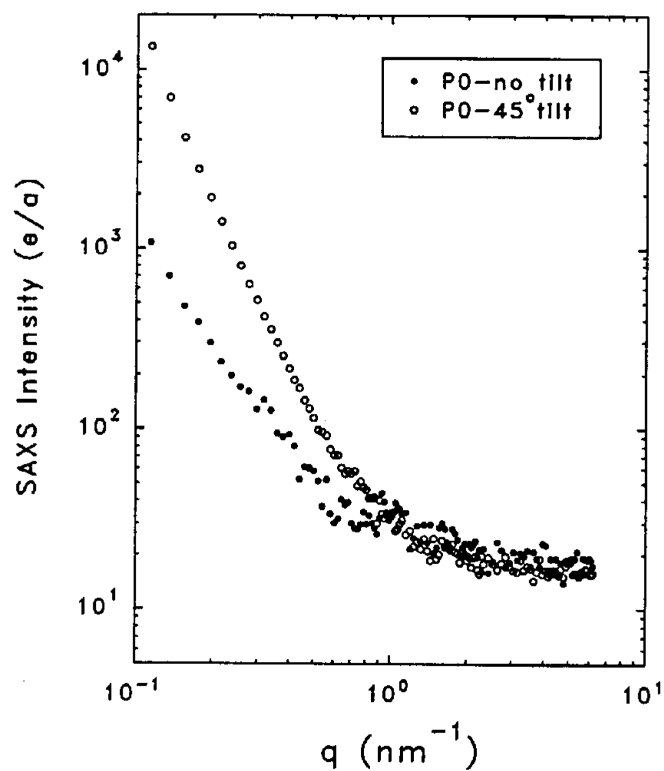

Fig. 3. Effect of tilting of sample on SAXS intensity of an IACS He-diluted film.

3.1.5 Record Solar Cell Material

We requested and received three films from USSC that were prepared under nominally the same conditions of each of the three intrinsic layers of their recent world record efficiency solar cell [8], an a-Si:H top layer and a-SiGe:H middle and bottom layers. The SAXS data from the three layers are shown in Fig.4. The a-Si:H top layer yields a fit (solid line) consistent with only a power-law rise at low q due to some large-scale features (>20 nm) and a constant diffuse intensity due to the compositional and static disorder. If any nanovoids are present they must be at a level of 0.01 vol.% or less. This behavior of the top-layer material is typical of the best device-quality a-Si:H investigated by SAXS in the past. The two Ge-containing layers show much stronger SAXS (Fig.4). The Ge contents were obtained by EPMA at NREL and found to be 40 at.% for the middle cell and 50 at.% for the bottom cell. Discussions with USSC confirm that the 40% value is higher than expected. The actual device has grading of the Ge content and the films made for SAXS were made with a single composition meant to represent the average Ge in the layer. Thus, the data from the middle cell may not be representative of the actual device.

The increased SAXS from both a-SiGe:H layers is due to nanostructural features on the 2 nm size scale. Assuming spherical objects, the average radius for the middle layer is 2.2 nm and for the bottom layer is 1.8 nm. In order to make a more meaningful comparison of the a-Si:H top layer and the a-SiGe:H bottom layer, the data are normalized to the same electron density contrast and the same diffuse intensity and compared in Fig.5. On this linear q scale, the dramatic difference in degree of heterogeneity is clear. The features are also elongated and oriented as determined from SAXS tilting experiments. A summary of the SAXS data from the three layers is provided in the following table.

Table 3. SAXS results from USSC triple-junction solar cell i-layers

Sample	composition	Q_N (10^{24} eu/cm^3)	I_d (eu)	A (eu/nm^3)	<R> (nm)	Q(0°)/Q(45°)
L9278	a-Si:H	≤0.02	10	6.5	a	3.3
L9280	a-$Si_{0.6}Ge_{0.4}$:H	4.7	72	23	2.2	b
L9279	a-$Si_{0.5}Ge_{0.5}$:H	9.4	67	9	1.8	5.3

a. Signal too weak to determine size.

b. Not measured.

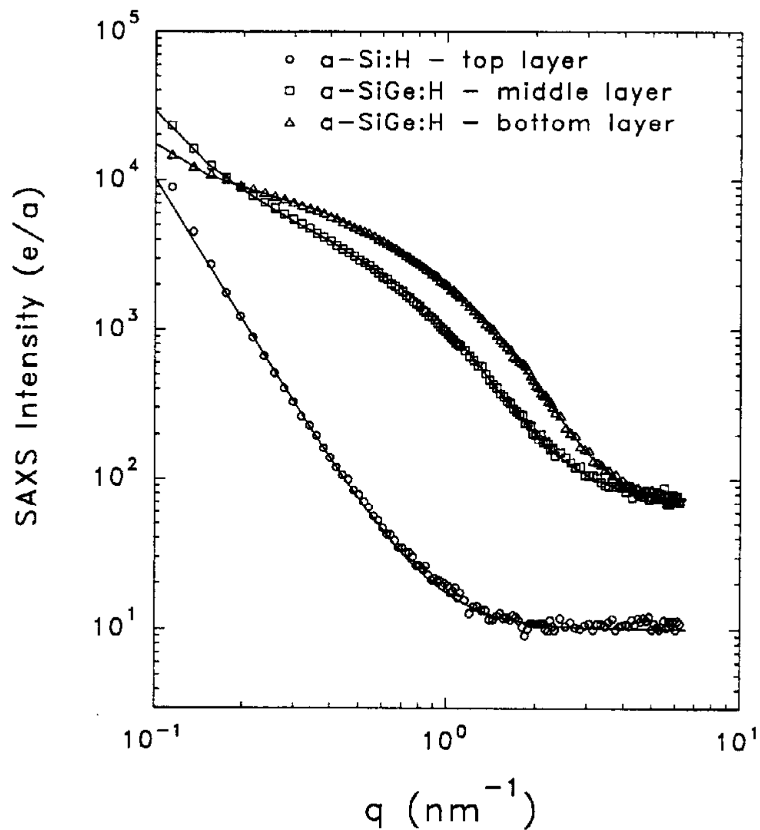

Fig. 4. SAXS from USSC films prepared to represent the three intrinsic layers of the recent triple-junction, world record efficiency device [8].

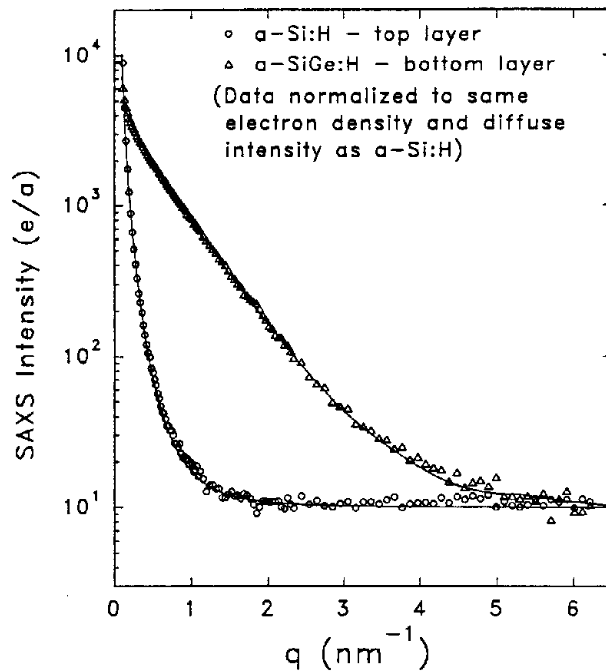

Fig. 5. More direct comparison of SAXS from top layer (a-Si:H) and bottom layer (a-$Si_{0.5}Ge_{0.5}$:H) by normalizing to the same electron density and diffuse intensity.

3.1.6 Hotwire Deposition

The NREL group has successfully grown high quality a-$Si_{1-x}Ge_x$:H alloys by the hotwire chemical vapor deposition technique using silane and germane gas mixtures [9]. These alloys display opto-electronic properties as good as those grown by PECVD but these hotwire films are grown at much higher deposition rates - up to 4 nm/s. Similar to hotwire a-Si:H, elevated substrate temperatures (375°C) lead to improved properties. A systematic set of alloys covering the range from x=0 to x=1 was prepared for SAXS analyses. Since Al foil substrates were used for the SAXS films, the elevated substrate temperatures sometimes led to Al-induced crystallization [10] so care was taken to characterize each sample by x-ray diffraction and new samples were grown at slightly lower substrate temperatures to avoid this effect. Table 4 summarizes all of the hotwire samples prepared for SAXS, their substrate temperatures, and whether they showed some crystallinity. They are ordered according to x as determined by EPMA.

Table 4. Hotwire a-$Si_{1-x}Ge_x$:H alloys prepared for SAXS study. T_{hc} is the temperature of the heater can which is approximately 125°C larger than the actual substrate temperature. The "u" and "d" refer to the upstream and downstream ends of the sample, respectively.

Sample	GeH_4(%)	x	T_{hc}(°C)	crystallinity	Preparation comments
HGe71	0	0	500	weak	
HGe83	0	0	492	none	
HGe82	0	0	490	mod-u	50% H_2 dilution
HGe103	0	0	475	none-u	50% H_2 dilution
HGe102	3	0.06	475	none	
HGe76	3	0.09	500	mod-u/weak-d	
HGe100	8	0.13	475	none-u	
HGe80	8	0.14	500	weak-u	
HGe106	17	0.19	486	none	on c-Si substrate
HGe73	17	0.23	500	none	
HGe75	35	0.28	500	none	
HGe74	35	0.38	450	none	
HGe72	35	0.41	500	strong-u	
HGe84	70	0.77	485	strong-u	
HGe104	70	0.79	400	none	
HGe77	100	1	350	none-u/strong-d	

The deposition geometry was asymmetric such that the filament was located closer to one end of the substrate than the other. The gas flow direction was such that the downstream end was the end closer to the filament. The samples were sectioned into 3 parts: a downstream (d) end, a middle part (used for EPMA) and an upstream (u) end. The d and u ends were analysed separately by SAXS due to large differences in deposition rates (~0.5 to 1 nm/s on the u end and 2 to 3 nm/s on the d end). Some differences were also detected in the degree of crystallinity on the d and u ends as noted in Table 4.

Example SAXS data and fitting results are shown in Figures 6-8 where one can see a dramatic change in the nature of the SAXS as x changes from 0 (Fig. 6) to 0.13 (Fig. 7) to x=0.23 (Fig. 8). One can observe the obvious stronger SAXS from the d end materials which experienced the larger deposition rates. The solid lines through the data are fits of spherical particle size distributions shown in the lower plots of each of the figures. The x=0 material has a wide distribution of sizes up to at least 15 nm. Larger sizes (> 15 nm) are present as detected by needing significant Porod terms, A/q^3, to fit the continuously rising signal at lower q. For x=0.13 one can already see a transition to a loss of the larger features and for x=0.23 (and 0.19), the size distribution has a well-defined upper limit near 5 nm and the Porod term is near zero. This behavior persists for all higher x values as summarized in the results for all samples in Table 5. Note the average radii decrease from near 4 nm at x=0 to less than 2 nm for x>0.19.

Examination of the data in Tables 4 and 5 allows one to conclude that the effect of the crystallinity on the SAXS is a contribution to the Porod slope (A), indicating that the microcrystals are in the size range greater than 15 nm (radius). This can be seen best from the samples HGE82, 76, 72, 84, and 77. Thee larger <R> values for HGe84 are likely due to some influence of the strong crystallinity. It is interesting to note that the relatively large A values for the x=0 material are not due to crystallinity since no crystallinity was found in HGe83 and it was weakly detected in HGe71.

Figure 9 shows the systematics of the integrated SAXS, Q_N, versus x for all the hotwire a-$Si_{1-x}Ge_x$:H alloys. Note the systematically higher Q's for the d end materials and the sharp rise around x=0.1. This transition to much more microstructure is similar to our earlier result for PECVD material [11], however, in the latter case the transition occured near x=0.2. The effect of hydrogen dilution was apparently to delay this transition to even larger x (~0.4) [1]. The data for HGe106, grown on c-Si rather than Al foil (Fig. 8, Table 5 and Fig. 9) show that the Al-foil substrate is not causing the change in microstructure. For convenient comparison, Fig. 9 shows the size of the Q's expected for various fraction of voids. Included in Fig. 9 are the data from the USSC microwave materials (Table 1) and the USSC record solar cell materials (Table 3). Note the ability of the high substrate bias to dramatically reduce the Q (2 data points below the 0.01 % void line) and the similarity of the low bias Q's to those of the hotwire a-$Si_{1-x}Ge_x$:H alloys.

Also, the record solar cell materials have Q's quite similar to those of the hotwire a-$Si_{1-x}Ge_x$:H alloys for the middle and bottom layers (x=0.4 and 0.5).

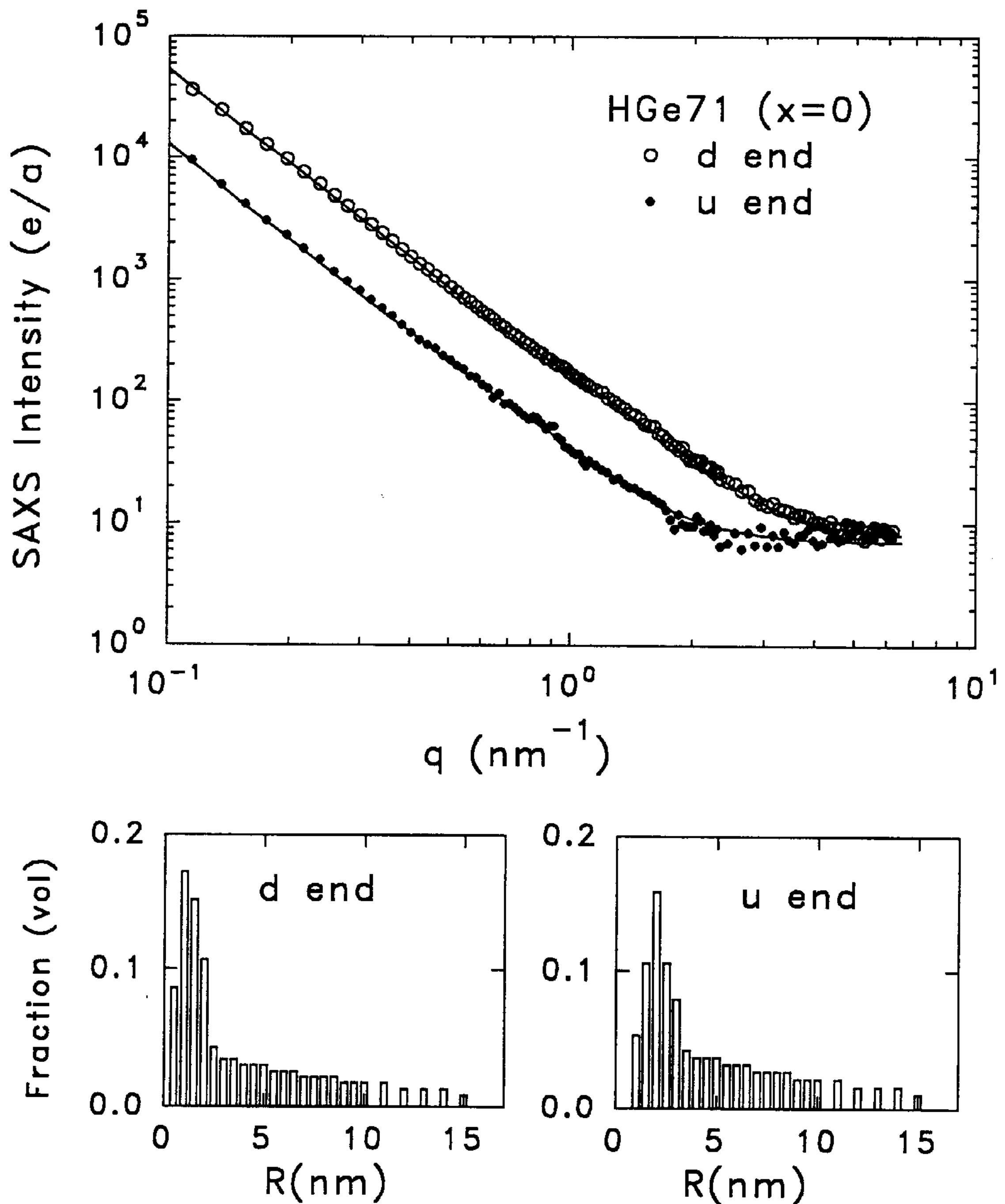

Fig. 6. SAXS from hotwire a-$Si_{1-x}Ge_x$:H alloy (x=0 in this case). Lower graphs show size distributions of spheres used to generate the solid lines (which includes a q^{-3} Porod term and a constant diffuse term, I_d) through the data in the upper graph.

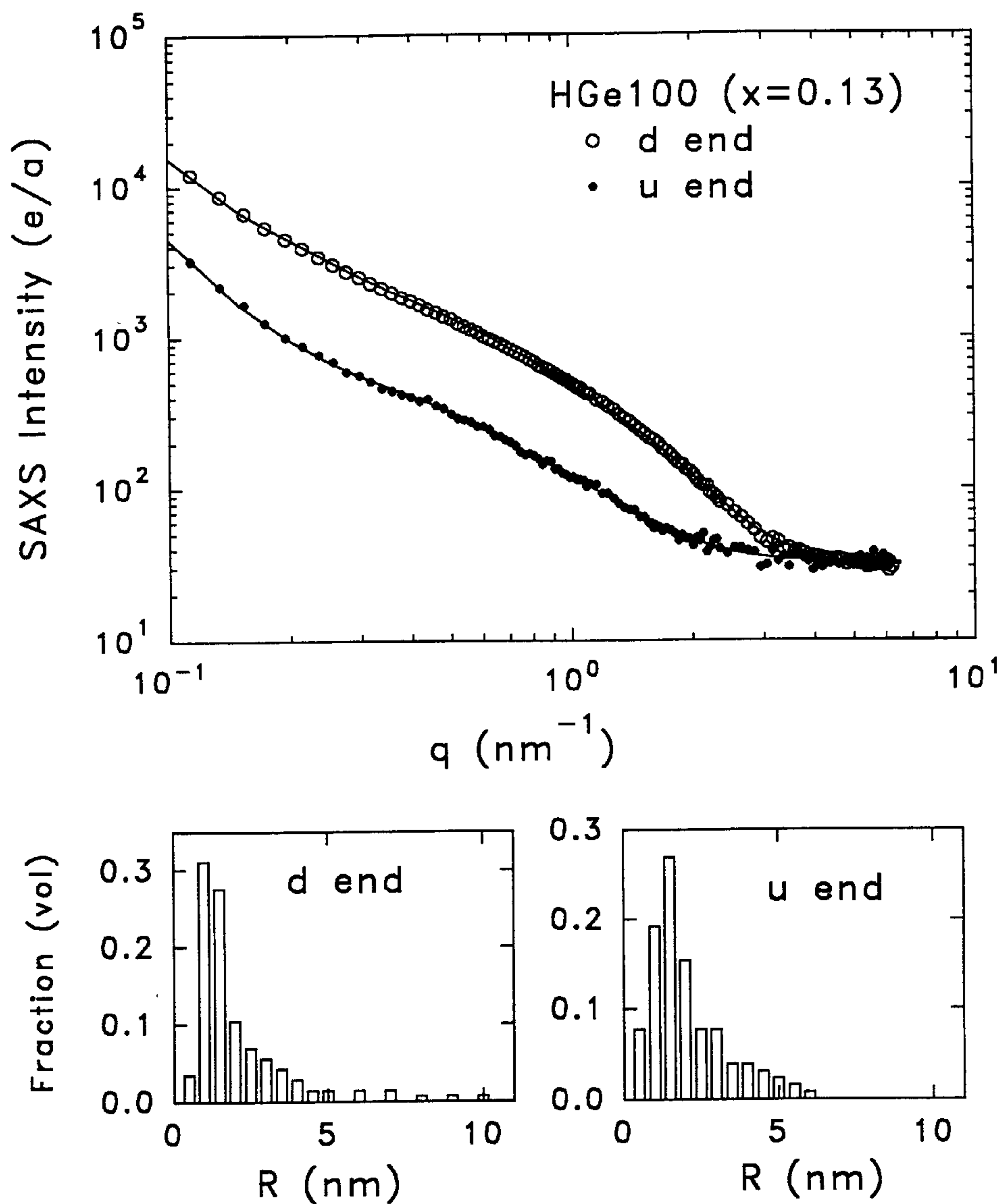

Fig. 7. SAXS from hotwire a-$Si_{1-x}Ge_x$:H alloy (x=0.13 in this case). Lower graphs show size distributions of spheres used to generate the solid lines (which includes a q^{-3} Porod term and a constant diffuse term, I_d) through the data in the upper graph.

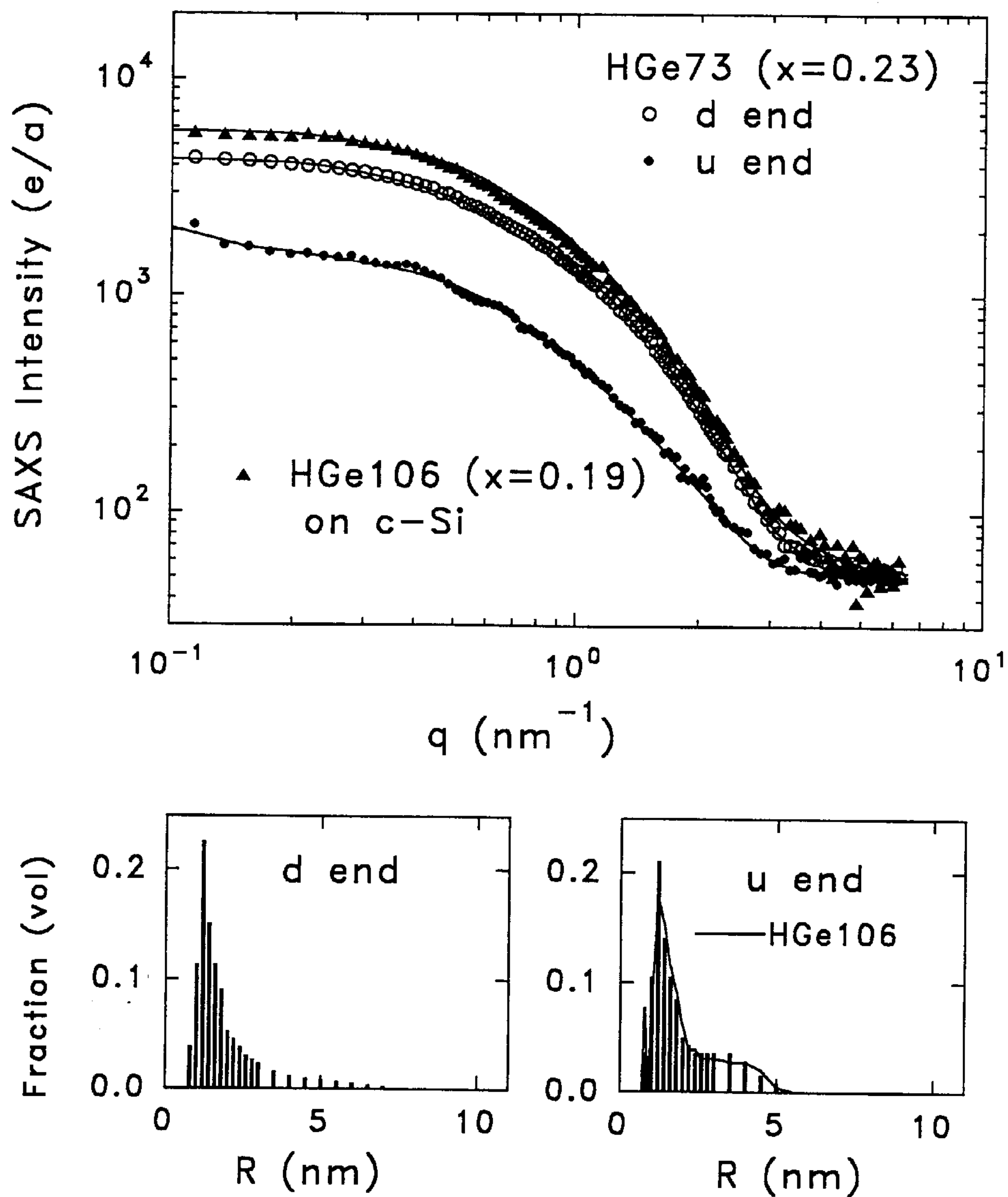

Fig. 8. SAXS from hotwire a-$Si_{1-x}Ge_x$:H alloys (x=0.19 and 0.23 in this case). Lower graphs show size distributions of spheres used to generate the solid lines (which includes a q^{-3} Porod term and a constant diffuse term, I_d) through the data in the upper graph.

Table 5. SAXS results for hotwire a-$Si_{1-x}Ge_x$:H alloys. The results for the d and u ends of each sample are provided. Sample HGe106 is on c-Si and has only one region investigated.

Sample	x	Q_N(u)	Q_N(d)	A(u)	A(d)	I_d(u)	I_d(d)	<R>(u)	<R>(d)
		(10^{24}eu/cm^3)		(eu/nm^3)		(eu)		(nm)	
HGe71	0	0.17	0.86	12	50	7	7.5	4.7	3.8
HGe83	0	0.064	0.70	11.5	50	8.5	9	3.6	3.4
HGe82	0	1.5	3.7	26	7.5	9	6	1.7	2.6
HGe103	0	0.81	2.5	1	10	9	8	2.8	1.7
HGe102	0.06	0.11	1.45	6	45	25	24	3.3	3.7
HGe76	0.09	0.060	0.68	55	19	26	23	3.0	2.2
HGe100	0.13	0.43	2.4	4	12	32	30	2.0	2.1
HGe80	0.14	1.2	4.3	28	5.5	38	36	2.0	1.8
HGe106	0.19	7.8		0		50		1.8	
HGe73	0.23	2.0	5.9	0.5	0	48	48	1.8	1.7
HGe75	0.28	3.2	17	0.4	1	56	51	1.6	1.5
HGe74	0.38	12	21	0	1.5	62	58	1.6	1.7
HGe72	0.41	7.1	20	65	28	66	60	1.8	1.7
HGe84	0.77	19	40	65	45	47	52	5.7	4.0
HGe104	0.79	22	32	4	4	50	50	2.3	1.9
HGe77	1.00	40	32	0	175	32	18	2.7	2.6

We also investigated the orientation of the microstructure of several of the hotwire a-$Si_{1-x}Ge_x$:H alloys by performing tilting SAXS experiments. The results are listed in Table 6 where one can see that all of the alloys show some preferred orientation of the scattering objects as revealed by Q ratios different from unity. As observed many times in the past, such ratios are consistent with elongated features (voids or H-rich objects) with their long axis parallel to the growth direction and therefore consistent with columnar-like growth. There is an absence of a tilt effect for the Porod term (A) except for the x=0 material. This can be interpreted that the microcrystalline material induced by Al substrate interdiffusion has no preferred orientation, while the larger features in the x=0 films are clearly oriented. Thus it appears that some residual columnar-like growth occurs for the x=0 material on a rather large scale (> 15 nm).

A correlation of the SAXS with the opto-electronic properties of the hotwire a-$Si_{1-x}Ge_x$:H alloys has been presented and discussed in reference 9.

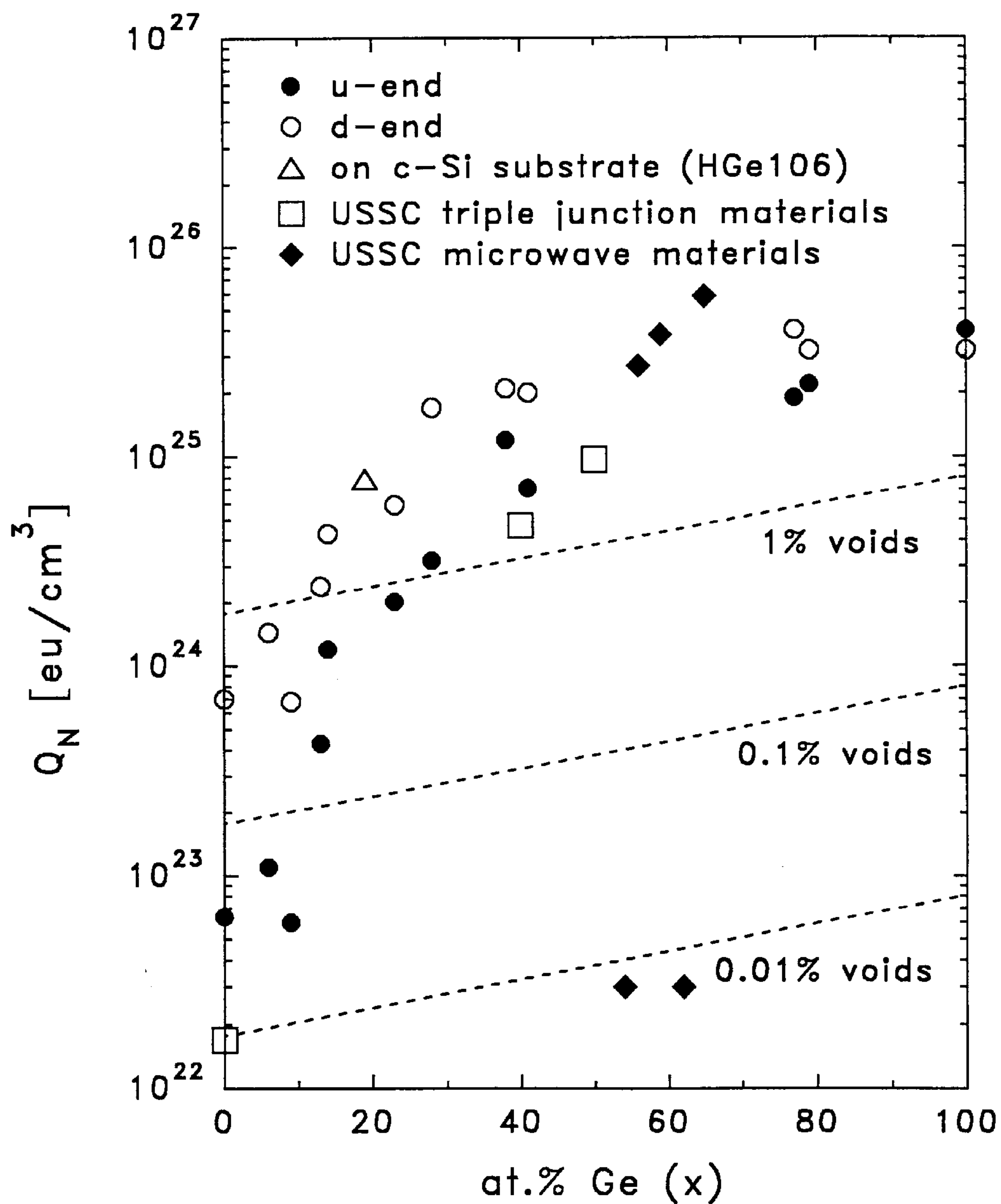

Fig. 9. Integrated SAXS intensities from hotwire a-$Si_{1-x}Ge_x$:H alloys and USSC PECVD a-$Si_{1-x}Ge_x$:H alloys (Data from Tables 1,3, and 5).

Table 6. Results of SAXS tilting experiments for several hotwire a-$Si_{1-x}Ge_x$:H alloys.

Sample	x	position	$Q_N(0^o)/Q_N(45^o)$	$A(0^o)/A(45^o)$
HGe71	0	u-end	2.9	1.1
		d-end	2.0	7
HGe83	0	u-end	1.5	8
HGe76	0.09	u-end	≥2	1.1
HGe80	0.14	u-end	4.3	~1
HGe73	0.23	u-end	5.3	~1
		d-end	5.4	~1
HGe75	0.28	u-end	1.9	~1
HGe74	0.38	u-end	4.9	~1
HGe72	0.41	u-end	4.0	1.0
HGe77	1.00	u-end	3.0	~1

3.1.7 Ge Uniformity

Several a-$Si_{1-x}Ge_x$:H alloys prepared by different PECVD techniques with x~0.5 to 0.7 show clear evidence of inhomogeneous distributions of Ge by ASAXS. The size scale of the inhomogeneity is characterized by a model with a correlation length parameter which varies from only 1.0 to 1.4 nm for the different samples. This non-uniformity is removed by enhanced ion bombardment during growth and it is reduced by hydrogen dilution of the plasma. The anisotropic ASAXS from the Ge is consistent with Ge enrichment along columnar-like nanostructures. The samples studied to date include the PECVD material prepared by IACS for the SAXS study described in section 3.1.1 and in Ref. 1 and the microwave PECVD material prepared by USSC for the SAXS study described in section 3.1.3. In both cases, the improved Ge homogeneity correlated with better opto-electronic or device properties. The details of the technique and the results are presented in Ref. 12.

3.1.8 Thermal Stability

There has been very little research on the thermal stability, hydrogen solubility, and hydrogen diffusion in a-$Si_{1-x}Ge_x$:H alloys. From our considerable collection of alloys received for prior SAXS studies in the as-deposited state, we have selected a set of six alloys prepared by three groups (USSC, Harvard, Stuttgart) as shown in the table below.

Table 7. Alloys selected for thermal stability study.

SAMPLE	T_s (°C)	x	H (at.%)
USSC#2092 (low bias)	400	0.59	7
USSC#2093 (high bias)	400	0.54	10
Harvard#420 (non-optimized)	200	0.73	20
Harvard#423 (optimized)	200	0.75	16
Stuttgart#111 (lower Ge)	200	0.20	6
Stuttgart#191 (higher Ge)	200	0.32	6

This set was systematically annealed at different temperatures and times to examine the following effects on thermal stability:

a) Ge content (samples range from x=0.2 to 0.75);

b) H content (samples range from 6 to 20 at.%H)

c) Initial (as-deposited) nanostructure (samples range from no detectable nanovoids to significant volume fractions with columnar-like features)

Details of the experiments and the analyses are reported elsewhere [13]. Some of the results are as follows. Figure 10 compares the SAXS from the Harvard #420 film in the as-deposited state and after the last anneal. The increased SAXS is due to nanovoids (or H_2-induced nanobubbles) with diameters of only 2 nm. The reduced SAXS at high q is due to the reduced diffuse scattering from the much lower H in the amorphous matrix (i.e., the H has left the sample or accumulated as H_2 in the nanobubbles). Figure 11 shows a very different annealing-induced structural change: the SAXS has *decreased* compared to the as-deposited state of the high-deposition-rate USSC #2092 film (4 nm/s), suggesting an improvement in homogeneity upon annealing. The USSC film deposited under high bias was extremely stable as shown in Fig. 12.

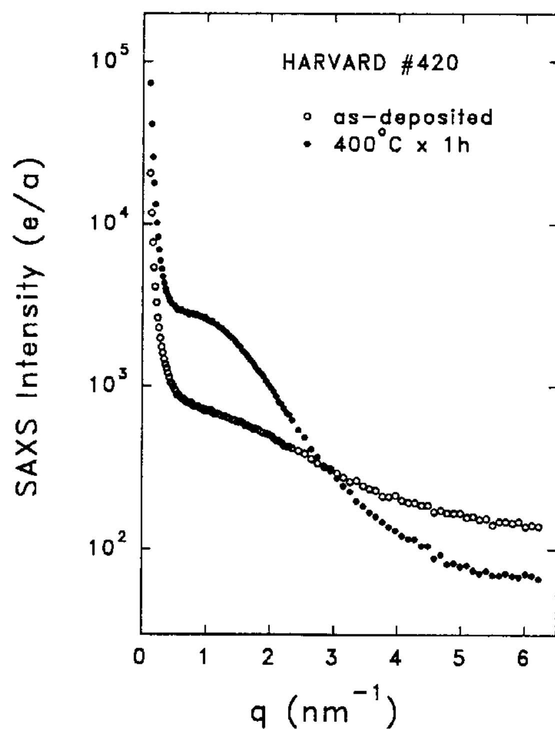

Fig. 10. SAXS data from annealing study of Harvard a-$Si_{1-x}Ge_x$:H sample.

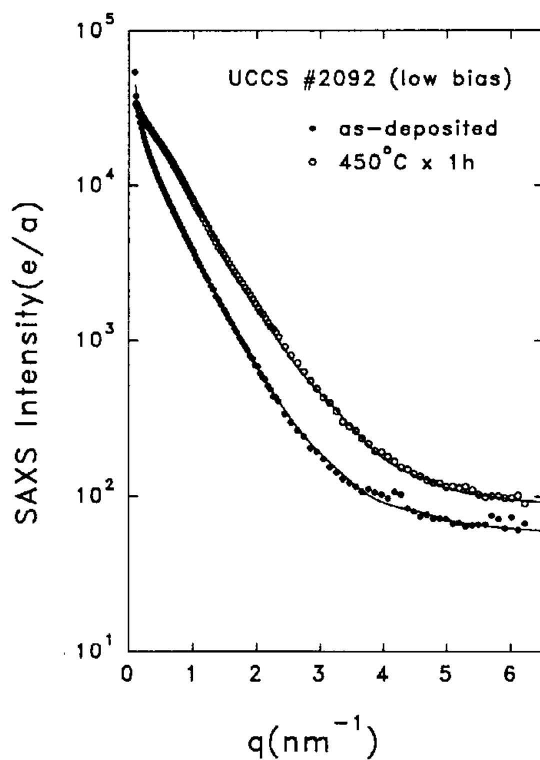

Fig. 11. SAXS data from annealing study of USSC a-$Si_{1-x}Ge_x$:H sample.

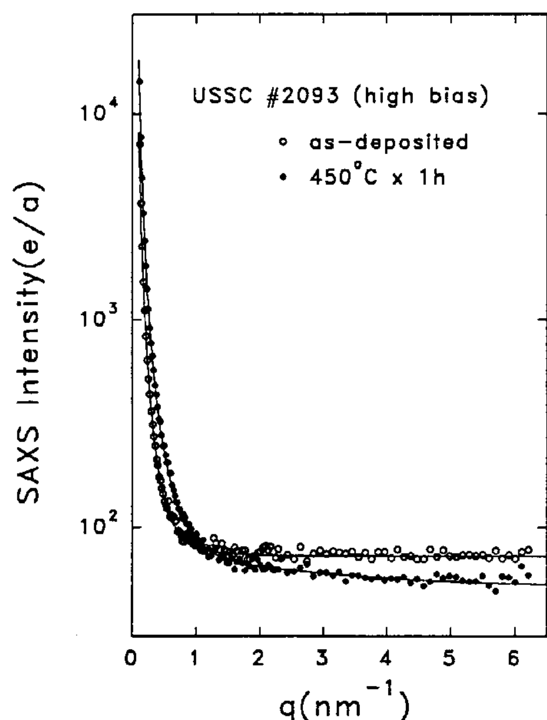

Fig. 12. SAXS data from annealing study of USSC a-$Si_{1-x}Ge_x$:H sample.

An overview of the results for the USSC and Harvard samples is shown in Fig. 13 by plotting the integrated SAXS intensities (Q). The vertical dashed lines indicate where a time series was initiated before going to the next 50°C or 25°C increment. The data points following the dashed lines are for 2 h, 4 h, 8 h, etc. anneals. Note that the drop in SAXS for the USSC #2092 begins at the lowest anneal temperatures, well below the T_s of 400°C. Figure 14 shows the systematic behavior of the diffuse SAXS intensity induced by H clustering and loss from the amorphous matrix. Finally, the sizes of the nanovoids and nanobubbles grow dramatically in the two Stuttgart films but to a much smaller extent in the other films as shown in Fig. 15.

These results may be of interest in the fabrication of solar cells. The a-SiGe:H alloy may be the first intrinsic layer deposited at 200 - 400°C. During deposition of the subsequent layers of the multijunction device, i.e., a-Si:H and a-SiC:H, an annealing process takes place at the substrate temperature and can affect the alloy in ways demonstrated by this study. In particular, if excess H above the solubility limit is included in the a-SiGe:H layer, then significant microstructural defects are induced. However, as shown for the USSC #2092 sample having poor initial microstructure, some improvement may occur during growth of the remaining cell layers.

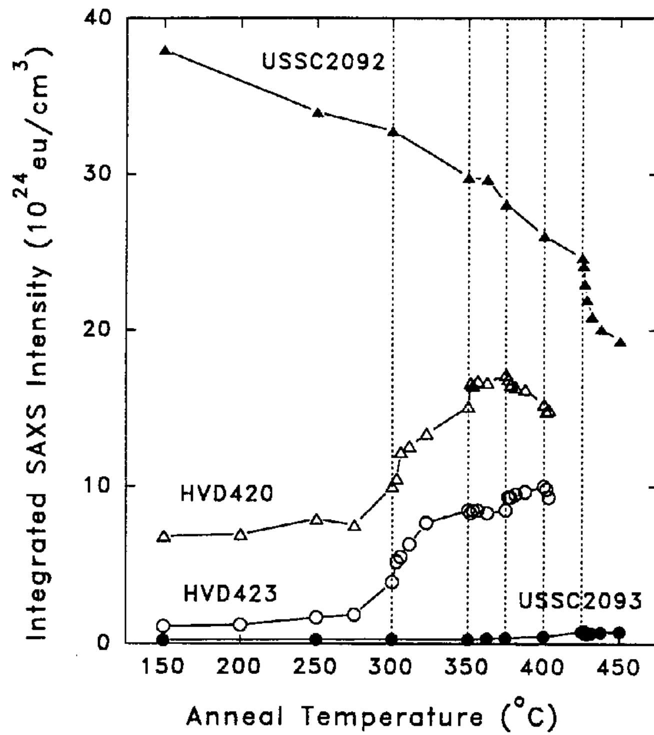

Fig. 13. Overview of annealing study results from USSC and Harvard samples.

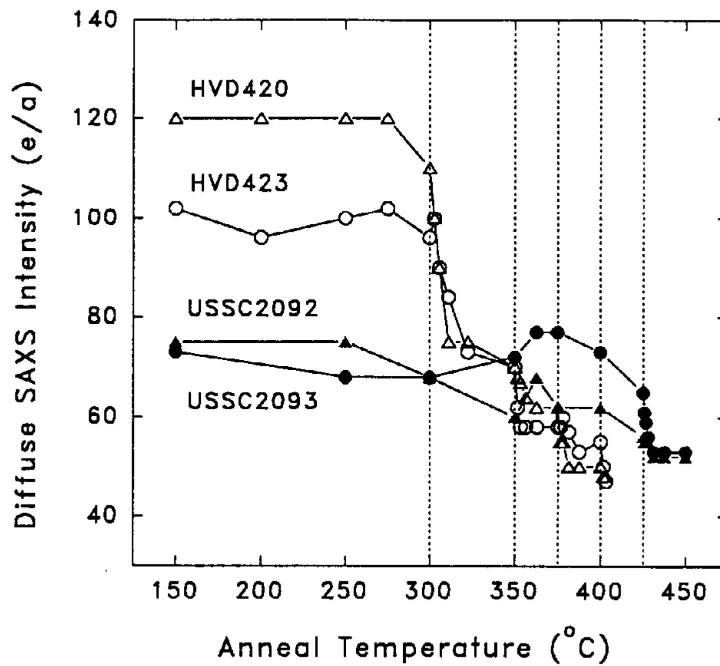

Fig. 14. Diffuse SAXS intensities versus annealing.

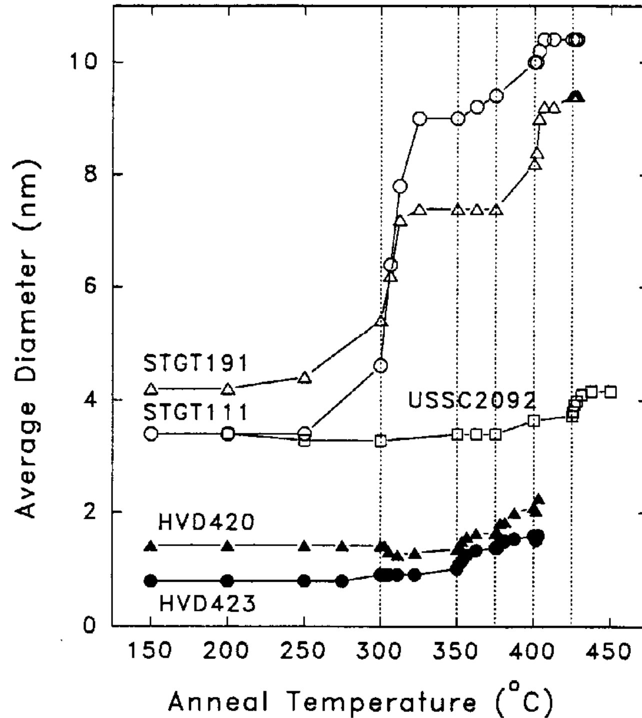

Fig. 15. Average diameter of scattering features from SAXS data versus annealing.

3.2 MID-GAP MATERIALS

3.2.1 Absolute Intensity and Device-Quality a-Si:H

The method for converting the SAXS intensity data to an absolute intensity scale in electron units was developed and checked by measuring the intensity from standard materials including H_2O [2,14] and $Al_{1-x}Ga_x$ alloys [15]. This allowed a determination of a lower detection limit for microvoids in a-Si:H with the in-house SAXS system of 0.01 vol.% [2,14]. Most device-quality a-Si:H films (i.e., that yield high efficiency solar cells, ~10%) show SAXS intensities near or below this detection limit. Examples of results for several PECVD films made by USSC, Solarex, APS and NREL are presented in the 1995 NREL annual report [14].

3.2.2 Staebler-Wronski Effect

Four high-quality a-Si:H films were selected for another look at possible changes in the nanostructure induced by light soaking. An early study by the CSM group found no evidence for light-induced changes[16] but our techniques have improved and a more careful procedure was developed. All four samples (listed in Table 8) were relatively thick and showed void fractions below or near our detection limit. All four samples were first annealed at 180ºC for 2 hours and then subjected to light soaking under 1 Sun for 1000 hours to place the samples in the degraded

Table 8. a-Si:H films selected for the Staebler-Wronski effect study.

sample	source	thickness	comments
S940304-71	NREL	4.5 μm	made by PECVD with no H_2 dilution - yields best cells
THD-76	NREL	2.3	made by Hotwire with conditions that yield best cells
B751	APS	3.0	made by PECVD with conditions that yield best cells
304181	EcolePoly	3.4	made by PECVD with H_2 dilution - $5x10^{15}$ defect density

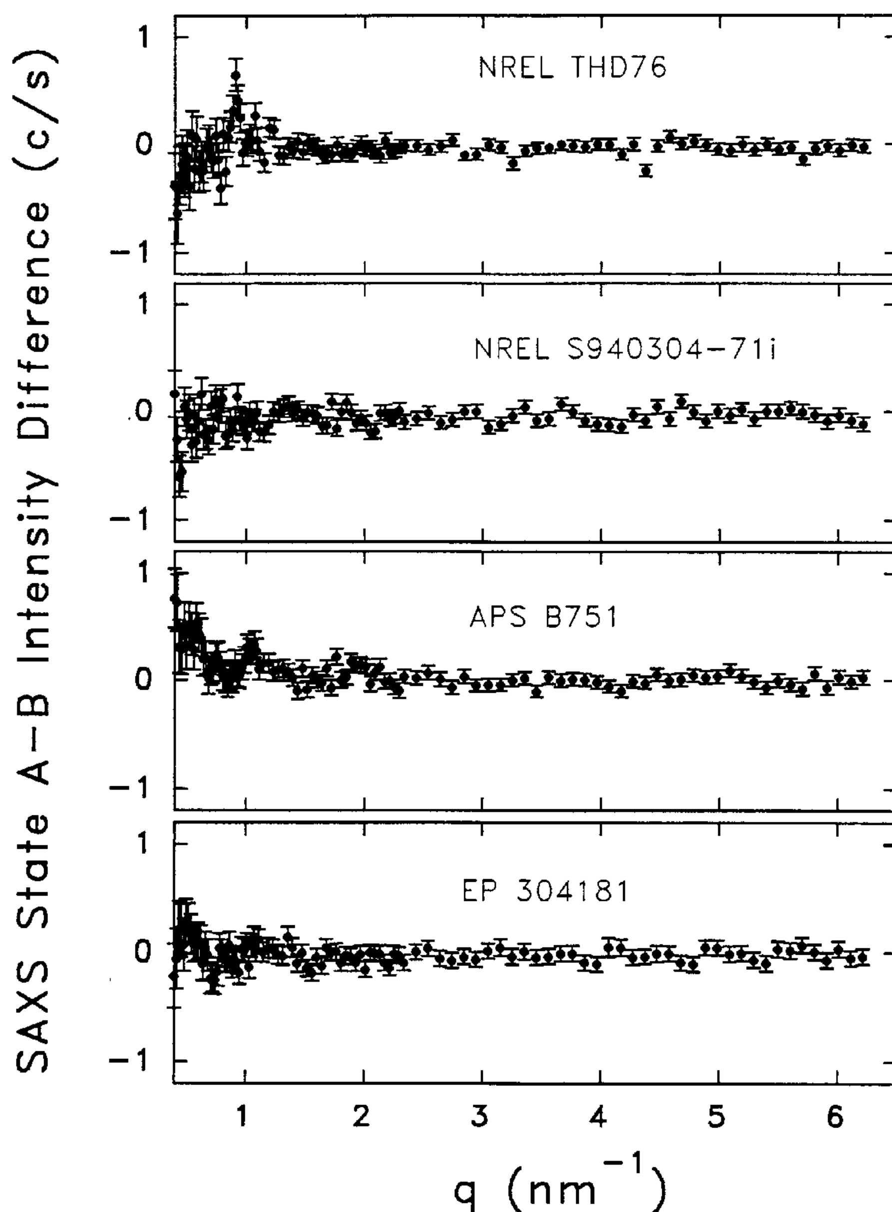

Fig. 16. SAXS data comparing states A and B via in-situ annealing method.

state B. SAXS measurements were then made in this state followed by in-situ annealing in the SAXS system to place each sample in state A. This allowed careful comparison of the SAXS in the two states by simply taking a difference in count rate at each q. Figure 16 shows the results from all samples. The error bars become larger at lower q since we are taking differences of larger and larger numbers. The average deviations from zero (for the q-range from 0.4 to 6.2 nm^{-1}) for the four sample are all below 0.1 count/s and three are negative and one is positive. Thus it is concluded that there is no significant difference in the nanostructure as determined by SAXS between states A and B of the Staebler-Wronski effect.

3.2.3 Model a-Si and a-Si:H

A reproducible form of a-Si can be prepared by ion implantation of c-Si with Si ions. This can be followed by H implantation to produce material of controlled H content at selected depths into the a-Si. SAXS studies demonstrated that the a-Si is completely free of voids and any other inhomogeneity on the nanometer scale and that such a-Si is stable with respect to void formation up to 540°C [17]. Based on these results, one can conclude that the known density deficit of 1.8% relative to c-Si must be due to an average increase in bond length in the a-Si [17]. Studies of the a-Si:H samples [18] demonstrated a solubility limit of 3 to 4 at.% H. Concentrations above this level led to H clustering and nanobubble formation upon annealing above 300°C. The growth of the nanobubbles was measured by SAXS to begin near 1 nm after a 350°C anneal and increase to 3 nm after a 550°C anneal. The size was confirmed by direct TEM observation [19]. A detailed comparison of ion-implanted a-Si:H and PECVD a-Si:H with similar H contents (11 at.%) shows that they behave quite differently upon annealing [20,21]. The PECVD sample shows much less clustering of H suggesting a higher solubility of H. Details of these investigations can be found in references 17-21 and in the Ph.D. thesis of S. Acco [22].

3.2.4 Device-Quality Hotwire Material

The a-Si:H hotwire material developed by NREL for solar cells is typically deposited at elevated substrate temperatures and has much less H than device-quality PECVD material. SAXS shows that this low-H material has less than 0.01 vol.% nanovoids and has a smaller diffuse scattering component consistent with the smaller concentration of H [2]. Thus, both PECVD and hotwire device-quality a-Si:H materials have undetectable quantities of nanovoids. Both types of material have some larger-scale features that cause SAXS at the smallest angles [2].

The NREL hotwire film THD76, made under device-quality conditions (~375°C), with low H content (~3 at.%), has been systematically annealed and characterized by SAXS. Its flotation density was also measured to be 2.29 g/cm^3, the highest density yet measured for a-Si:H. This same film was used in the light-soaking study described in Section 3.2.2. The purpose here was

to search for any diffusion-induced changes in nanostructure that might occur due to the unusually high diffusion coefficient for H in hotwire a-Si:H material [23]. The sample, 2.3 µm thick, was fully characterized in the as-deposited state, light-soaked state, and the 200°C annealed state and no differences were detected. This series of six scans was averaged to obtain a high precision reference before the series of higher temperature anneals, all of which were below the deposition temperature of 375°C.

The SAXS results are shown in Fig. 17, where it is clear that some changes occurred upon annealing under the indicated conditions. First, it needs to be made clear that the initial nanostructure is nearly homogeneous and the subsequent changes are very small, but apparently real. The data can be fitted with a sum of 3 contributions to the intensity versus q due to (a) nanostructural features (<5 nm), I_N, (b) larger structural features (>20 nm), I_L and (c) a q-independent diffuse background, I_D [2]. The as-deposited sample has a maximum nanovoid volume fraction of 0.005 % based on a maximum integrated signal (Q) from I_N, while the diffuse component is only I_D=3.7 e/a, a low value consistent with the low H content. This value seems to drop somewhat upon annealing at 300°C as seen from more data points below those of the as-deposited sample at high q. Such a drop would be expected as the H leaves the bonding sites and clusters or leaves the sample, thereby reducing the Si-H Laue monotonic scattering. An interesting result is the slope of the data at low q corresponding to the I_L term: this is fitted with A/q^s where s = 4.2. Such a high value is very different from the s = 3 expected from simple Porod behavior in a line focus SAXS system. Upon annealing one can see that the slope changes at low q and fits give $s = 3.5 \pm 0.1$ for all the annealed states. In addition there is a small but clear appearance of a contribution to I_N corresponding to features about 2 nm in radius, corresponding to a volume fraction of nanovoids of 0.01%. The Porod slope is known to be affected by the diffuseness/sharpness of the boundaries between phases of a two-phase system and this is being examined as a possible explanation of the large values of s.

3.2.5 Ar Dilution

Nanostructural heterogeneity of a-Si:H deposited by conventional PECVD, but under Ar dilution has been characterized by SAXS and several opto-electronic methods [24]. There is a minimum in the amount of heterogeneity near 90% Ar dilution and this shows a strong correlation with a minimum in the Urbach energy and the defect density determined by dual-beam photoconductivity. Evidence for a two-phase microstructure is found above 90% dilution and microcrystallinity develops at 99% Ar dilution and higher plasma power. Details are available in reference 24.

3.2.6 Boron Doping

Doping of PECVD a-Si:H via 1%TMB in He leads to dramatic increases in the nanovoid density as determined by SAXS [25]. Undoped a-Si:H yielded a 0.04% nanovoid volume fraction and this increased systematically with B doping, reaching a 2.1% volume fraction of 1

nm diameter voids at the highest doping level. These results were used in a study that demonstrated red-orange light emission from anodically etched porous a-Si:H, clearly demonstrating that crystallinity is not a requirement for light emission. The intensity of the PL peak at ~2.2 eV correlates well with boron concentration and nanovoid density in the starting a-Si:H film. We propose that anodic pore formation is seeded on nanovoids in the a-Si:H layer [25].

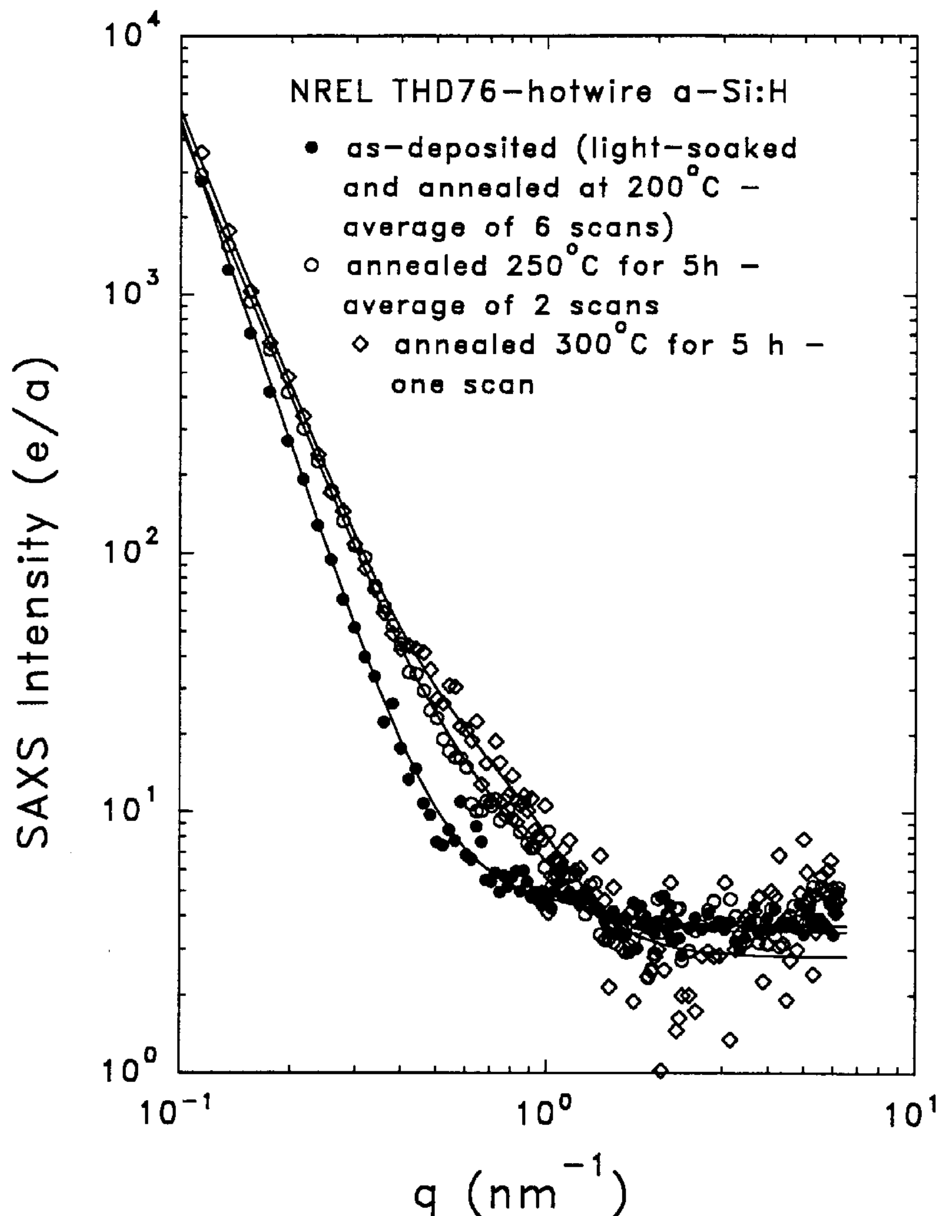

Fig. 17. Effect of annealing on the nanostructure of hotwire a-Si:H.

3.2.7 Medium-Range Order and Microcrystallinity

Conventional wide-angle x-ray diffraction (XRD) in the symmetric Bragg-Brentano mode has been found to yield useful information from on the order of 1-micron-thick a-Si:H and microcrystalline Si films[26-28]. Medium-range structural order is probed by examining the full-width-at-half-maximum (FWHM) intensity of the lowest angle diffraction peak (near 28 degrees 2θ). A series of hotwire samples prepared at increasing substrate temperature was found to have a systematic decrease in the FWHM suggesting improved medium-range order and a possible correlation with improved stability of the hotwire material with low H content [26]. The FWHM of this first XRD peak is found to decrease even more when the films become partially microcrystalline as readily detected by the appearance of the (111), (220), and (311) XRD peaks of c-Si. The width and relative intensities of the latter peaks vary depending on deposition conditions and these features have been used to estimate crystallite sizes (~10-30 nm) and preferred grain orientations in hotwire films [27] and hotwire solar cells [28].

3.2.8 Record Solar Cell Material

The USSC record efficiency device [8] has an intrinsic a-Si:H layer that was duplicated on Al foil for SAXS study. This material has an undetectable nanovoid fraction (<0.01% based on the Q_N value in Table 3) but a clear signal due to larger-scale structure that rises steeply at the lowest angles (see Fig. 4). This behavior is similar to all device-quality a-Si:H films that yield the best solar cells. Note that this is in sharp contrast with the behavior of the a-$Si_{1-x}Ge_x$:H alloys used for the other layers of the triple junction cell described in Section 3.1.5.

3.3 HIGH-GAP MATERIALS

3.3.1 Microvoid Density in a-SiC:H

Analysis of several a-$Si_{1-x}C_x$:H alloys prepared by different groups with x from 0.07 to 0.27 yields similar results [2]: high densities (1-2 vol.%) of voids that are spherical or randomly oriented and only about 1 nm in diameter. Hydrogen dilution does reduce the nanovoids somewhat, but no a-$Si_{1-x}C_x$:H alloy has been examined yet that does not show a strong characteristic SAXS signal due to the above features. In addition, there is always a broad maximum or a shoulder in the SAXS data that indicates interparticle interference that is never seen in the a-Si:H or a-$Si_{1-x}Ge_x$:H alloys. The interference can be modeled by an effective interaction such that the nanovoids are correlated in position, possibly due to a strain field associated with each nanovoid [2].

3.3.2 ECD High V_{oc} a-Si:H Material

A film of a-Si:H prepared with the same conditions used as an i-layer in single junction cells with initial V_{oc} = 1.04 V and stabilized V_{oc} = 1.01 V at ECD was received for structural

characterization. Figure 18 shows the very weak SAXS from the ECD sample. For comparison the expected SAXS from 0.1% voids of average radius 2 nm is shown. The signals from the ECD sample are clearly much less than this. Also, the SAXS at low q shows little or no tilt effect so this larger-scale structure (surface roughness?) has no preferred orientation. Standard x-ray diffraction measurements showed no evidence of microcrystallinity.

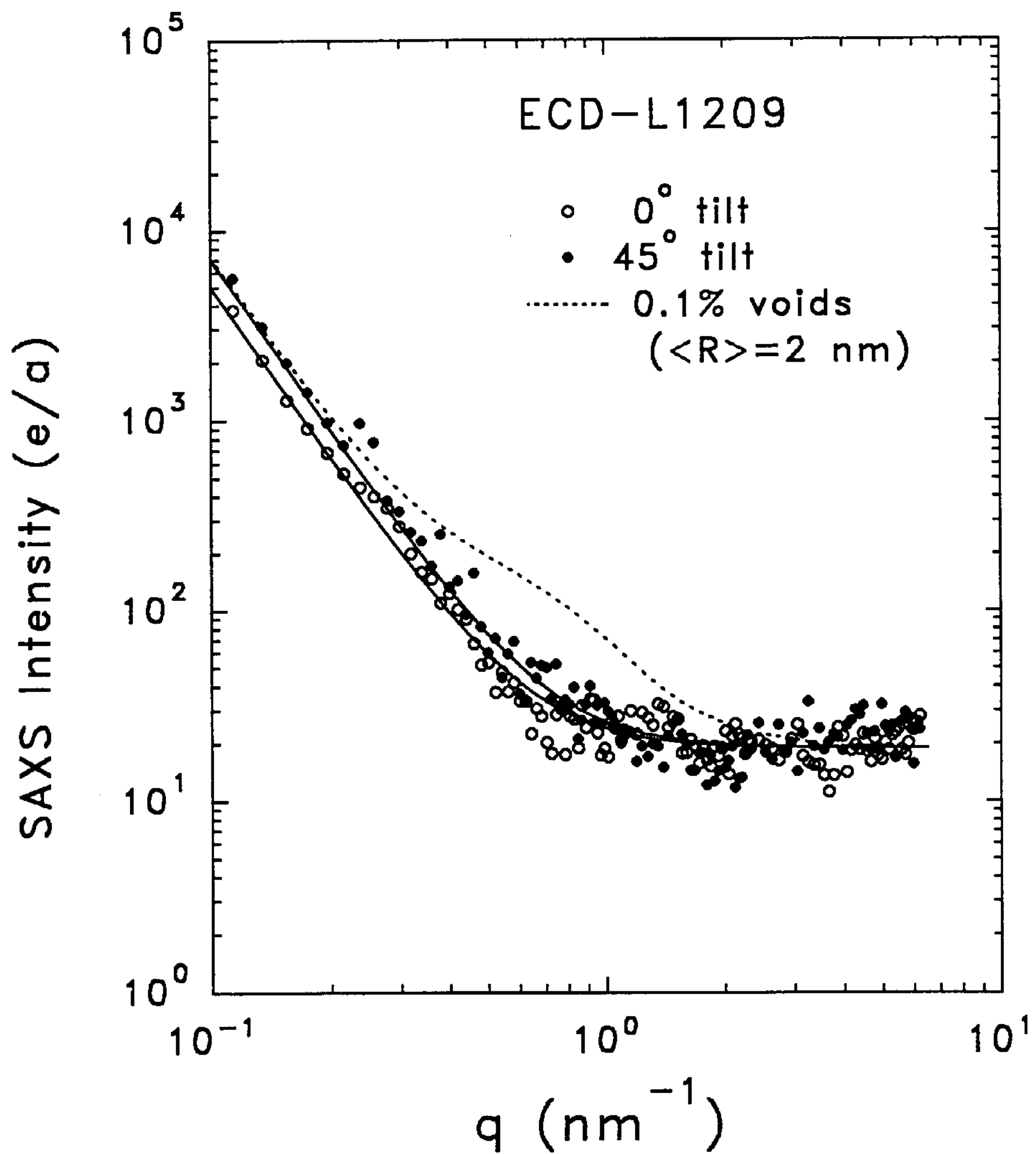

Fig. 18. SAXS from ECD a-Si:H, high V_{oc} material.

The x-ray absorption data yield a film thickness of 0.8 microns. This is thinner than our typical samples and is the cause of the observed scatter in the data. In addition to the SAXS film on Al-foil (L1209), flakes were provided that came loose from films on glass due to poor adhesion and another film on glass (L1204) that was also coming loose from the substrate. Flotation density measurements were made on all three samples with the following results: L1209 (on Al foil) - 2.166 g/cm^{3}; L1204 (on glass) - 2.162 g/cm^{3}; flakes in vial - 2.162 g/cm^{3}. Since our uncertainty is about ±0.005 g/cm^{3}, there is no difference in the film density for the two types of substrates. However, this density is significantly lower that typical device-quality PECVD material (2.22-2.25 g/cm^{3}). Based on our density data versus H content, the above values are consistent with a total H content of about 18 at.%. This is also consistent with the diffuse scattering level of about 19 e/a which is about twice the level from samples containing 8-10 at.% H (see, e.g.the data from the NREL sample in Fig. 1 of Ref. 2 and the USSC a-Si:H data in Fig. 4). The lack of voids is a remarkable result for a sample with this high a hydrogen content.

3.3.3 TIT Chemical Annealing Material

Two series of films prepared by the "chemical annealing" method [29,30] at the Tokyo Institute of Technology (TIT) have been investigated. Five samples were made with various ratios of T1 (time for deposition) and T2 (time for hydrogen-plasma treatment), all at the low substrate temperature of 100°C. The second set of 4 samples was deposited at various substrate temperatures. Defect densities were measured to be less than 10^{16}/cm^{3} and there is evidence of increased stability for this high-gap material [31]. The SAXS samples, deposition conditions, and known properties are listed in Table 9.

Series #1 Analyses

We became suspicious of the strong SAXS signals from some of the samples so we checked for microcrystallinity by x-ray diffraction (XRD) and found three of the films to be at least partially microcrystalline. It was discovered that we could distinguish the microcrystalline areas by a different appearance: grayish versus redish colors - the grayish = microcrystalline (μc) and redish = amorphous (probably due to the higher bandgap of the amorphous areas). This is documented by the XRD patterns in Fig. 19 for the five samples. The sharp peaks are from the Al-foil substrate. We find: AR74 - uniform appearance and amorphous; AR76 - about 50% of area is redish (labeled "r" on Fig. 19) and 50% is grayish (labeled "g" on Fig. 19 - the Miller indices of the μc-Si are indicated); AR77 - uniform appearance and microcrystalline; AR78 - about 70% of area is redish and about 30% is grayish; AR79 - uniform appearance and amorphous.

Table 9. Deposition conditions and properties of TIT high optical gap a-Si:H films.

sample	substrate T (°C)	Dep. rate (nm/s)	Thickness (μm)	T1(s)/T2(s)	Optical gap (eV)	H-content (at.%)
Series # 1						
AR74	100	0.170	2.14	continuous	1.75	12.1
AR76	100	0.184	1.76	10/20	2.01	21.3
AR77	100	0.139	1.39	10/40	2.05	11.1
AR78	100	0.150	1.80	20/40	2.02	22.2
AR79	100	0.180	1.80	10/10	1.91	17.1
Series # 2						
AR173	125	--	1.0	10/10	--	--
AR178	100	--	1.0	10/10	1.92	21.7
AR176	75	--	1.0	10/10	--	--
AR177	50	--	1.0	10/10	1.94	23.9

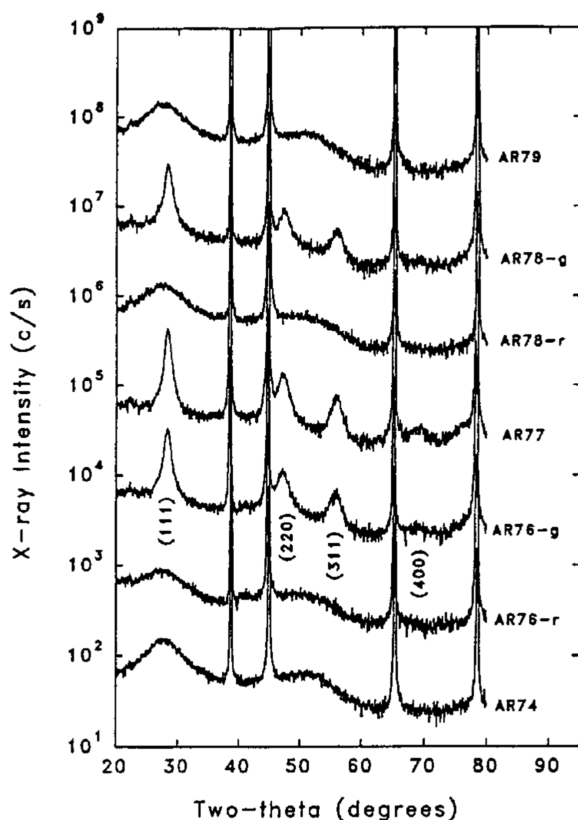

Fig. 19. Standard x-ray diffraction data from TIT series #1 films.

Based on the widths of the μc peaks we estimated the crystallite sizes (L) using the Scherrer equation: for sample AR77 - L(111) = 8.0 nm, L(220) = 4.6 nm, and L(311) = 5.3 nm. (The AR76 and 78 samples look similar in linewidth to AR77).

After discovering the different μc-Si and a-Si:H regions we were careful to distinguish which parts of the film were used for the density measurements. Table 10 gives the results which we believe are accurate to ±0.005 g/cm^3.

Table 10. Flotation density results for TIT series #1 samples.

Sample	appearance (structure)	density (g/cm^3)
AR74	uniform (a-Si:H)	2.149
AR76-r	redish (a-Si:H)	1.994
AR76-g	grayish (μc-Si)	2.122
AR77	uniform (μc-Si)	2.134
AR78-r	redish (a-Si:H)	1.937
AR78-g*	grayish* (μc-Si)	2.070*
AR79	uniform (a-Si:H)	2.042

(*we think this piece also included some of the redish amorphous phase)

Thus one can see that the μc-Si tends to be more dense although the fully-amorphous AR74 is more dense than any of the samples or regions. Recall that the density of c-Si is 2.33 g/cm^3 so the density deficits range from 17% (AR78-r) to 8% (AR74). As will be seen from the SAXS, such large deficits are mostly due to H alloying.

Since each of the five samples was folded to make 8 layers, the mixed-structure samples (AR76 and AR78) yielded contributions from both μc-Si and a-Si:H. Figure 20 shows the SAXS intensities together with the data from a high-quality PECVD sample made at NREL [Fig. 1 in ref. 2]. The two fully amorphous samples (AR74 and AR79) yielded the weakest SAXS, while the fully microcrystalline sample (AR77) yielded the strongest SAXS. Consistent with these results, the mixed-structure samples yield signals in between. We observe decreases upon tilting AR74 and AR79 which is consistent with elongated scattering objects aligned parallel with the growth direction. The results of the SAXS analyses are provided in Table 11.

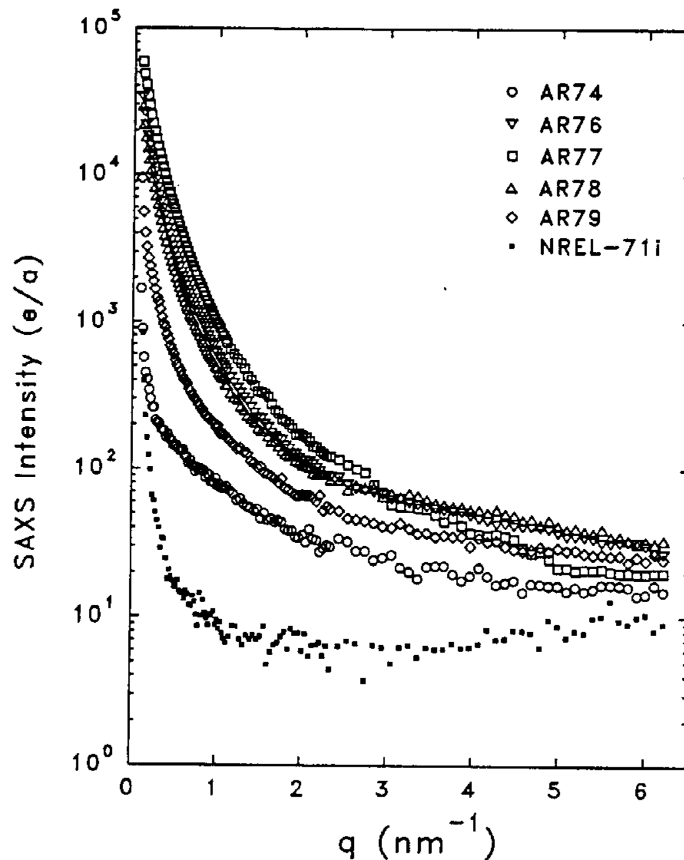

Fig. 20. SAXS from TIT series #1 a-Si:H films and from NREL device-quality film.

Table 11. SAXS results from TIT series # 1 samples.

sample	Q (eu/cm^3)	A (eu/nm^3)	I_d (eu)	<R>	Q_o/Q_{45}
AR74	4.3E23	1.2	14	1.2	3.1
AR76	4.4E24	22	23	3.3	
AR77	7.5E24	35	12	3.7	
AR78	3.5E24	20	26	3.2	
AR79	1.1E24	6	22	2.3	1.8

As can be seen, the integrated SAXS intensity, Q, is lowest for AR74, about a factor of two larger for AR79, and more than an order of magnitude higher for AR77. The A parameter is a measure of larger-scale microstructure (>20 nm) and seems to scale with Q. The volume-weighted average radius of the scattering objects, <R>, also seems to increase with Q. Note that the average diameter for AR77 is 7.4 nm and this is consistent with the crystallite sizes estimated above from the XRD peak widths. Thus the <R> is most likely related to the μc state for AR76-78, while for AR74 and 79 it is more likely a measure of nanovoid sizes. The tilt ratios Q_o/Q_{45}

for AR74 and 79 are both >1, consistent with elongated and oriented nanovoids in a columnar-like structure.

The values of the diffuse scattering intensity, I_d, correlate quite well with the amount of H in the films. This is reasonable since the diffuse scattering from a binary alloy will scale with alloy content [2].

We can estimate the maximum possible volume fraction of nanovoids in AR74 and AR79 using Eq. 4 of ref. 2 assuming n_p=0 (void) and n_m=n(c-Si)ρ(film)/ρ(c-Si), i.e. the electron density of the matrix is that of c-Si reduced by the ratio of flotation density of each film to the density of c-Si. We say this will be the "maximum possible" because the tilt ratio>1 says the scattering is anisotropic so the experimental Q is larger than the value expected from a sample with randomly-oriented voids. We find: AR74, f = 0.26 %; AR79, f = 0.75 %. Clearly these values do not account for the measured density deficits, which can be attributed mainly to the H alloying. However, these are quite high void fractions compared to typical device-quality a-Si:H (usually near 0.01%).

We can also estimate the volume fraction of μc-Si in AR77 assuming n_p=n(c-Si) and n_m= n(c-Si)ρ(a-Si:H)/ρ(c-Si), where ρ(a-Si:H) = [ρ(film)-fρ(c-Si)]/(1-f) and f is the μc volume fraction. We find: AR77, f=85 %. We are not sure how reliable this value is since it implies the density of the remaining amorphous fraction is only 1.02 g/cm^3. Anyway, the XRD data in Fig. 19 suggests it is predominantly microcrystalline.

Series #2 Analyses

This series of 4 samples was prepared with various substrate temperatures while other deposition conditions were fixed (Table 9). Figure 21 shows the data and fits for the samples in the untilted orientation. Figure 22 shows the strong effect of tilting one of the samples by 45 degrees. The drop in intensity indicates oriented, non-spherical scattering objects, probably associated with columnar-like growth. Table 12 shows all of the results of the measurements and analyses.

As can be seen from the data in the table, the results are quite systematic:

i) The flotation density decreases with decreasing substrate temperature.

ii) The integrated SAXS intensity (Q) increases with decreasing substrate temperature, corresponding to more scattering features (low-density H-rich regions or nanovoids).

iii) The ratio Q_o/Q_{45} increases with decreasing substrate temperature corresponding to more oriented scattering features.

iv) The average radius <R> (corresponding to the minor axis if ellipsoids assumed with long axes parallel to growth direction) remains between 2.2 and 2.8 nm.

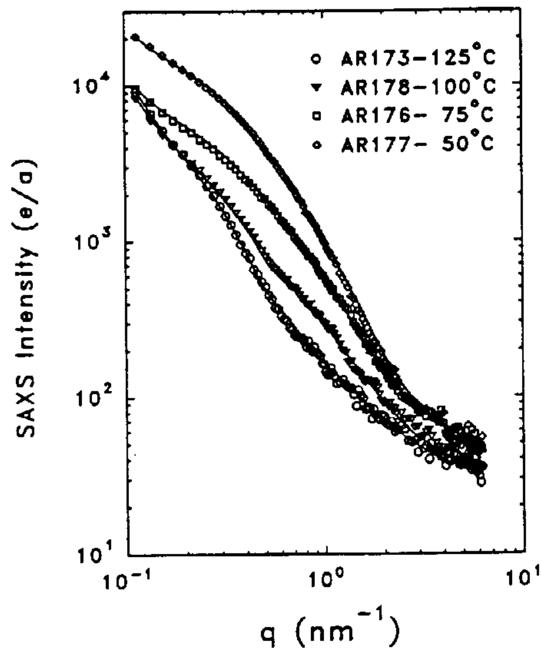

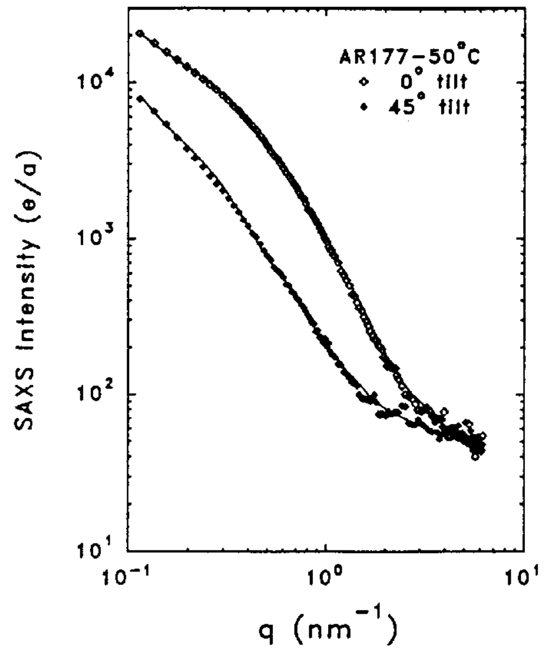

Fig. 21. (left) SAXS data from TIT series #2 films.

Fig. 22. (right) Effect of tilting on SAXS from one of the TIT series #2 films

Table 12. SAXS and flotation density results from TIT series # 2 samples.

Sample	ρ(flot) (g/cm^3)	Q ($10^{24}eu/cm^3$)	A (eu/nm^3)	I_d (eu)	<R> (nm)	Q_o/Q_{45}	f(max) (%)	f(cor) (%)
AR173	2.088	0.99	9	34	2.8	2.2	0.6	0.3
AR178	2.067	1.69	8	33	2.2	3.8	1.0	0.4
AR176	2.020	3.32	6	48	2.3	3.9	1.9	0.7
AR177	2.000	6.15	11	40	2.7	4.8	3.6	1.2

v) If the Q's are converted to void fractions then f(max) represents the maximum possible fraction (assuming zero electron density in the voids) neglecting the tilt effects. f(cor) represents void fractions based on the simple ellipsoidal model with the tilt ratio used to estimate the corrected void fractions.

Note that even the f(max) values are not able to account for the changes in flotation density and this is likely due to the increasing amounts of H incorporated at the lower substrate temperatures (Table 9).

None of these 4 samples showed any evidence of microcrystallinity according to XRD.

3.3.4 IACS Hotwire-Assisted PECVD Material

Films of a-$Si_{1-x}C_x$:H have been prepared at IACS by a hybrid hotwire/PECVD method to try to combine the advantages of both [32]. We have completed the SAXS and flotation density measurements of 4 samples which were quite thin (only one was greater than the recommended minimum of 1 micron) so the SAXS data are somewhat noisy. The data are shown in Fig. 23. The results appear systematic and consistent with other data as listed in Table 13. Electron microprobe measurements were done at NREL to obtain C and O contents. In the table the values of x are based on a-$Si_{1-x}C_x$:H alloy compositions, but also reported are atomic concentrations of oxygen which seem rather high.

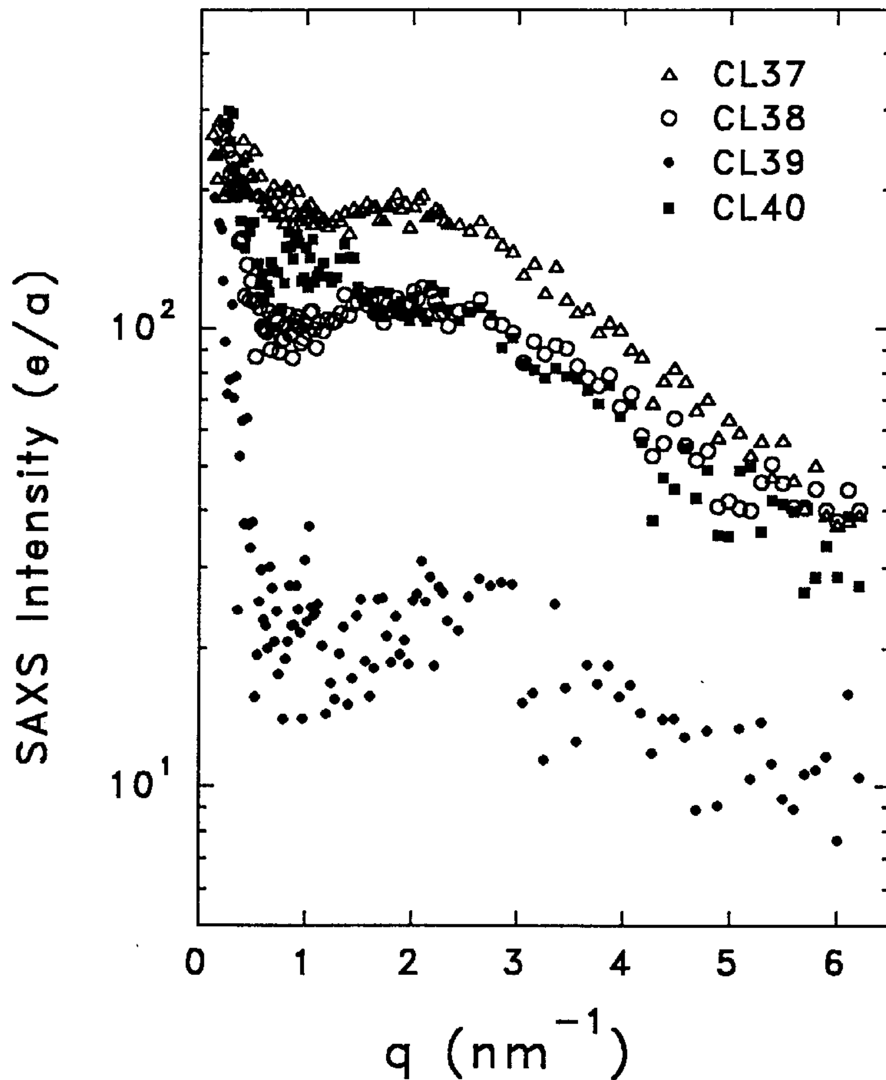

Fig. 23. SAXS data from IACS a-$Si_{1-x}C_x$:H alloys.

Table 13. Composition, SAXS, and flotation density results for IACS a-$Si_{1-x}C_x$:H

sample	thickness (μm)	x	O (at.%)	ρ(flot) (g/cm^3)	Q (10^{24}eu/cm^3)	I_d (eu)	<D> (nm)	f (vol.%)
CL37	0.6	0.070	5.2	1.97	3.3	30	1.1	2.4
CL38	0.8	0.065	3.3	2.10	1.8	30	1.4	1.2
CL39	1.2	0.008	1.4	2.23	0.2	10	~1.4	0.1
CL40	0.55	0.043	3.1	2.13	1.7	25	1.3	1.1

The results are similar to earlier observations of a-$Si_{1-x}C_x$:H alloys: even small amounts of C cause significant increases in the SAXS and the volume fractions of 1-nm-sized voids are near 1 or 2 % [2]. The low void fraction for CL39 is obviously associated with the low C content, although even this concentration leads to the characteristic shape of the SAXS scan for a-$Si_{1-x}C_x$:H alloys as seen in Fig. 23.

Although there is an apparent correlation between flotation density and Q (or f), it is clear that the density deficit is not due simply to the voids since the deficits (relative to c-Si) range from 4 % for CL39 to 15 % for CL37. Most of the deficit is very likely due to H alloying. The IACS group found evidence that the hotwire-assisted PECVD material was more stable after 100 h light soaking compared with conventional PECVD material [32].

3.3.5 Thermal Stability of a-SiC:H

A series of a-SiC:H alloys prepared by rf reactive sputtering by the Shinar group at Iowa State has been under systematic study to examine the thermal stability and H diffusion behavior. Figure 24 summarizes the annealing behavior of all the films. Compositions range from 2 to 7 at.%C. The behavior is quite similar for all films and demonstrates the formation of increased nanostructural features above 300°C. The time dependence of the increasing SAXS is shown in the lower portion of the figure for two different temperatures. The fits to the SAXS require the use of an interference model due to a high density of scattering centers or a position correlation effect as noted before [2]. Figure 25 clearly shows the increased numbers of nanovoids (or nanobubbles) with annealing and the data are fitted with radii of 0.55 nm for the as-deposited film and 0.65 nm for the annealed film. We associate this increased heterogeneity with H clustering. Details of this study can be found elsewhere together with with IR and SIMS

investigations of co-deposited samples[33].

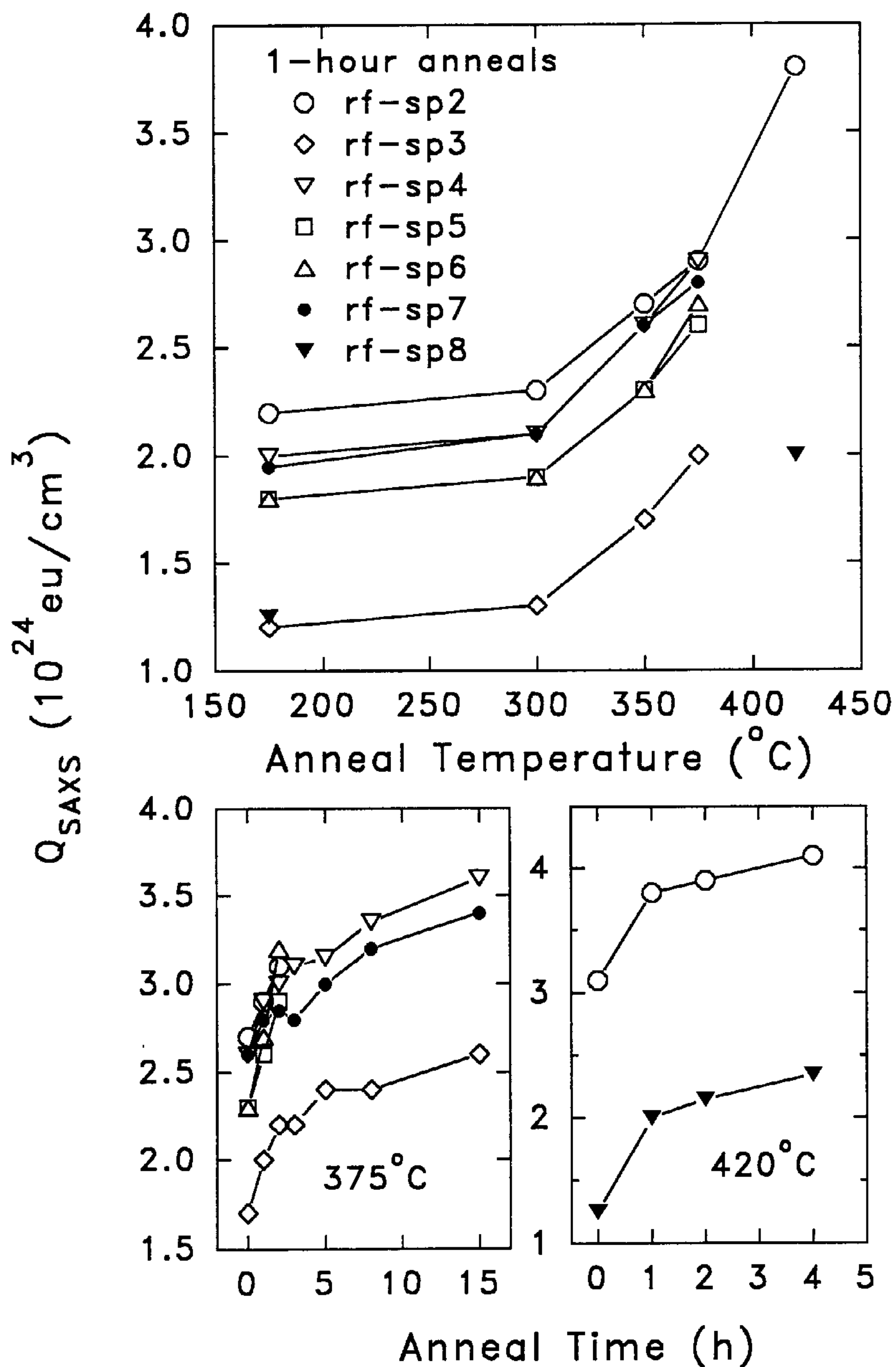

Fig. 24. Variation of the integrated SAXS intensities (Q) from a-SiC:H films versus anneal temperature and time.

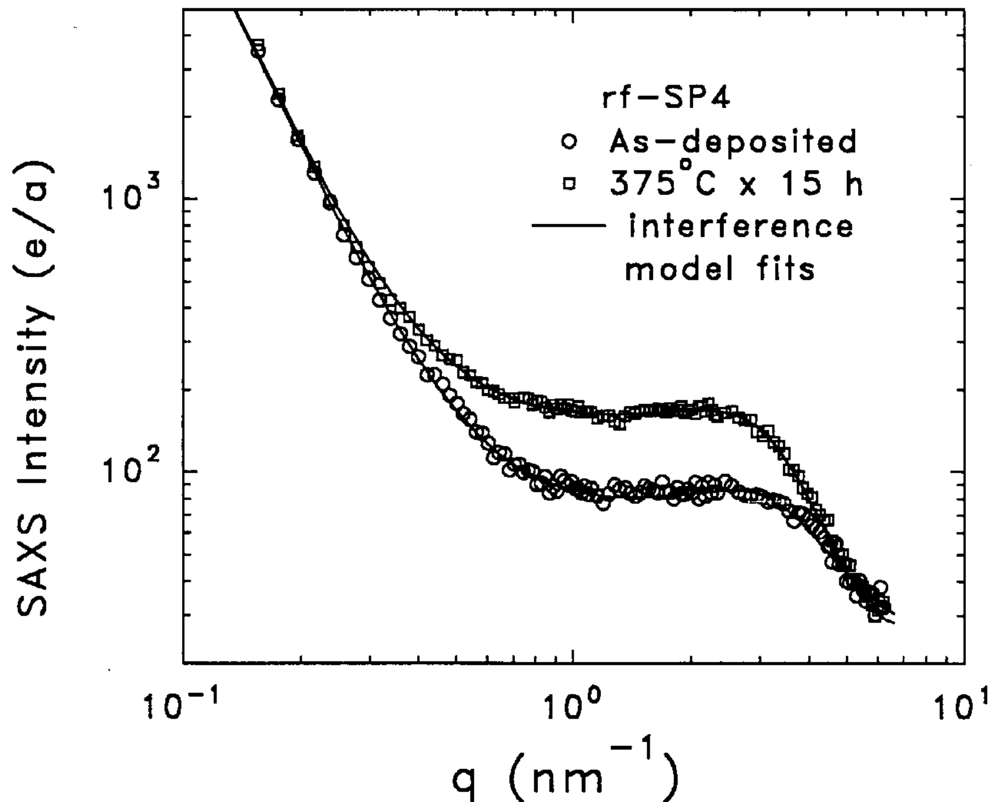

Fig. 25. Typical SAXS data from the Iowa State a-SiC:H alloys and the interference model fits.

4. REFERENCES

1. "Improvement of Microstructure of Amorphous Silicon-Germanium Alloys by Hydrogen Dilution", A.R. Middya, S. Ray, S.J. Jones and D.L. Williamson, J. Appl. Phys. **78**, 4966 (1995).

2. "Nanostructure of a-Si:H and Related Materials by Small-Angle X-ray Scattering", D.L. Williamson, Mater. Res. Soc. Symp. Proc. **377**, 251 (1995) [Invited paper for MRS Symposium on Amorphous Silicon Technology-1995].

3. "Recent Improvements in Glow Discharge a-$Si_{1-x}Ge_x$:H of Large x", P. Wickboldt, D. Pang, W. Paul, J.H. Chen, F. Zhong, C-C. Chen, J.D. Cohen, and D.L. Williamson, J. Appl. Phys. **81**, 6252 (1997).

4. S. Guha, X. Xu, J. Yang, and A. Banerjee, Appl. Phys. Lett. **66**, 595 (1995).

5. "Light-Induced Degradation of Amorphous Silicon-Germanium Alloy Solar Cells Deposited at High Rates", S. Sugiyama, X. Xu, J. Yang, and S. Guha, Mat. Res. Soc. Symp. Proc. **420**, 197 (1996).

6. S. Hazra, A.R. Middya, and S. Ray, J. Appl. Phys. **78**, 581 (1995).

7. S. Guha, Final Technical Progress Report, 1 August 1994 - 28 February 1998, NREL/SR-520-24724 (1995).

8. J. Yang, A. Banerjee, and S. Guha, Appl. Phys. Lett. **70**, 2975 (1997).

9. "Hydrogenated Amorphous Silicon Germanium Alloys Grown by the Hot-Wire Chemical

Vapor Deposition Technique", B.P. Nelson, Y. Xu, D.L. Williamson, B. von Roedern, A. Mason, S. Heck, A.H. Mahan, S.E. Schmitt, A.C. Gallagher, J. Webb, and R. Reedy, Mater. Res. Soc. Symp. Proc. (in press, submitted - 1998).

10. "Interdiffusion at a-Ge:H/Al and a-Si:H/Al Interfaces", S.J. Jones, A.B. Swartzlander-Franz, Y. Chen, and D.L. Williamson, Mat. Res. Soc. Symp. Proc. **297**, 1049 (1993).

11. "Microstructural Transition and Degraded Opto-electronic Properties in Amorphous SiGe:H Alloys", S.J. Jones, Y. Chen, D.L. Williamson, R. Zedlitz, and G. Bauer, Appl. Phys. Lett. **62**, 3267 (1993).

12. "Nanostructured Ge Distribution in a-SiGe:H Alloys from Anomalous Small-Angle X-Ray Scattering Studies", G. Goerigk and D.L. Williamson, Solid State Commun. (in press-1998).

13. "Microstructural Stability and Hydrogen Solubility in a-$Si_{1-x}Ge_x$:H", Nam Hyun Kang, Master of Science Thesis, Colorado School of Mines (1997).

14. "Microstructure of Amorphous-Silicon-Based Solar Cell Materials by Small-Angle X-ray Scattering", D.L. Williamson, Annual Subcontract Report, NREL/TP-411-8122 (1995).

15. "Alloy Diffuse Scattering Studied by Small-Angle X-ray Scattering", Dong-Hoon Min, Master of Science Thesis, Colorado School of Mines (1995).

16. D.L. Williamson, Y. Chen, S.J. Jones, and G.D. Mooney, Annual Report, Photovoltaic Subcontract Program FY 1991, NREL/TP-410-4724 (1992) p. 18.

17. "On the Nanostructure of Pure Amorphous Silicon", D.L. Williamson, S. Roorda, M. Chicoine, R. Tabti, P.A. Stolk, S. Acco and F.W. Saris, Appl. Phys. Lett. **67**, 226 (1995).

18. "Hydrogen Solubility and Network Stability in Amorphous Silicon", S. Acco, D.L. Williamson, P.A. Stolk, F.W. Saris, M.J. van den Boogaard, W. Sinke, W.F. van der Weg, S. Roorda and P. Zalm, Phys. Rev. B. **53**, 4415 (1996).

19. "TEM Observations of Hydrogen Nanobubbles in Implanted Amorphous Silicon", K.M. Jones, D.L. Williamson, S. Acco, and M.M. Al-Jassim, from *Proceeding of Microscopy and Microanalysis 1996*, Edited by G.W. Bailey (San Francisco Press, San Francisco, 1996) p.972.

20. "Structural Defects and Hydrogen Clustering in Amorphous Silicon", S. Acco, D.L. Williamson, S. Roorda, W.G.J.H.M. van Sark, A. Polman, and W.F. van der Weg, J. Non-Cryst. Solids **227-230**, 128 (1998).

21. "Nanoclustering of Hydrogen in Ion-Implanted and Plasma-Grown Amorphous Silicon", S. Acco, D.L. Williamson, W.G.J.H.M. van Sark, W.C. Sinke, W.F. van der Weg, A. Polman, and S. Roorda, Phys. Rev. B (submitted - 1998).

22. "Structural Defects and Hydrogen Clustering in Amorphous Silicon", Stefania Acco, Ph.D. Thesis, University of Utrecht (1997).

23. A.H. Mahan et al, Proc. 25th IEEE PV Spec. Conf., (1996) 1065.

24. "Nanostructures and Defects in Silicon Hydrogen Alloys Prepared by Ar Dilution", U.K.

Das, A.R. Middya, J.K. Rath, C. Longeaud, D.L. Williamson and P. Chaudhuri, Phil. Mag. (submitted - 1998).

25. "Visible Photoluminescence from Porous a-Si:H and Porous a-Si:C:H", M.J. Estes, L.R. Hirsch, S. Wichart, G. Moddel, and D.L. Williamson, J. Appl. Phys. **82**, 1832 (1997).

26. "Observation of Improved Structural Ordering in Low H Content, Hot Wire Deposited a-Si:H", A.H. Mahan, D.L. Williamson, and T.E. Furtak, Mater. Res. Soc. Symp. Proc. **467**, 657 (1998).

27. "Low Defect Density Microcrystalline-Si Deposited by the Hot Wire Technique", A.H. Mahan, M. Vanecek, A. Poruba, V. Vorlicek, R.S. Crandall, and D.L. Williamson, Mater. Res. Soc. Symp. Proc. (in press, submitted-1998).

28. "Microcrystalline Silicon n-i-p Solar Cells Deposited Entirely by the Hot-Wire Chemical Vapor Deposition Technique", Qi Wang, E. Iwaniczko, A.H. Mahan, and D.L. Williamson, Mater. Res. Soc. Symp. Proc. (in press, submitted -1998).

29. D. Das, H. Shirai, J. Hanna, and I. Shimizu, Jpn. J. Appl. Phys. **30**, L239 (1991).

30. H. Shirai, T. Ariyoshi, J. Hanna, and I. Shimizu, J. Non-Cryst. Solids **137-138**, 693 (1991).

31. M. Azuma, K. Nakamura, T. Yokoi, K. Yoshino, and I. Shimizu, Mat. Res. Soc. Symp. Proc. **377**, 191 (1995); K. Yoshino, K. Nakamura, and I. Shimizu, preprint.

32. D. Das, S. Chattopadhyay, and A.K. Barua, Solar Energy Materials and Solar Cells **51**, 1 (1998).

33. "Hydrogen Diffusion in Hydrogenated Amorphous Silicon Carbides", R. Shinar, J. Shinar, S. Mitra, F. Li, V.L. Dalal, and D.L. Williamson (in preparation - 1998).

REPORT DOCUMENTATION PAGE			Form Approved OMB NO. 0704-0188
Public reporting burden for this collection of information is estimated to average 1 hour per response, including the time for reviewing instructions, searching existing data sources, gathering and maintaining the data needed, and completing and reviewing the collection of information. Send comments regarding this burden estimate or any other aspect of this collection of information, including suggestions for reducing this burden, to Washington Headquarters Services, Directorate for Information Operations and Reports, 1215 Jefferson Davis Highway, Suite 1204, Arlington, VA 22202-4302, and to the Office of Management and Budget, Paperwork Reduction Project (0704-0188), Washington, DC 20503.			
1. AGENCY USE ONLY (Leave blank)	2. REPORT DATE November 1998	3. REPORT TYPE AND DATES COVERED Final Subcontract Report, 6 April 1994–30 June 1998	
4. TITLE AND SUBTITLE Microstructure of Amorphous-Silicon-Based Solar Cell Materials by Small-Angle X-Ray Scattering; Final Subcontract Report, 6 April 1994–30 June 1998			5. FUNDING NUMBERS C: XAN-4-13318-04 TA: PV905001
6. AUTHOR(S) D.L. Williamson			
7. PERFORMING ORGANIZATION NAME(S) AND ADDRESS(ES) Department of Physics Colorado School of Mines Golden, CO 80401			8. PERFORMING ORGANIZATION REPORT NUMBER
9. SPONSORING/MONITORING AGENCY NAME(S) AND ADDRESS(ES) National Renewable Energy Laboratory 1617 Cole Blvd. Golden, CO 80401-3393			10. SPONSORING/MONITORING AGENCY REPORT NUMBER SR-520-25844
11. SUPPLEMENTARY NOTES NREL Technical Monitor: B. von Roedern			
12a. DISTRIBUTION/AVAILABILITY STATEMENT National Technical Information Service U.S. Department of Commerce 5285 Port Royal Road Springfield, VA 22161			12b. DISTRIBUTION CODE
13. ABSTRACT *(Maximum 200 words)* This report describes work performed to provide details of the microstructure in high-quality hydrogenated amorphous silicon and related alloys for the nanometer size scale. The materials studied were prepared by current state-of-the-art deposition methods, as well as new and emerging deposition techniques. The purpose was to establish the role of microstructural features in controlling the opto-electronic and photovoltaic properties. The approach centered around the use of the uncommon technique of small-angle X-ray scattering (SAXS), which is highly sensitive to microvoids and columnar-like microstructure. Nanovoids of H-rich clusters with 1 to 4 nm sizes in a-Si:H at the 1 vol.% level correlate with poor solar-cell and opto-electronic behavior. Larger-scale features due either to surface roughness or residual columnar-like structures were found in present state-of-the-art device material. Ge alloying above about 10 to 20 at.% typically leads to significant increases in heterogeneity, and this has been shown to be due in part to non-uniform Ge distributions. Ge additions also cause columnar-like growth, but this can be reduced or eliminated by enhanced ion bombardment during growth. In contrast, C alloying typically induces a random nanostructure consisting of a narrow size distribution of 1-nm-sized objects with a high density, consistent with the notably poorer opto-electronic behavior of these alloys.			
14. SUBJECT TERMS photovoltaics ; microstructures ; amorphous-silicon materials ; small-angle X-ray scattering ; SAXS ; Ge alloying			15. NUMBER OF PAGES 51
			16. PRICE CODE
17. SECURITY CLASSIFICATION OF REPORT Unclassified	18. SECURITY CLASSIFICATION OF THIS PAGE Unclassified	19. SECURITY CLASSIFICATION OF ABSTRACT Unclassified	20. LIMITATION OF ABSTRACT UL

NSN 7540-01-280-5500

Standard Form 298 (Rev. 2-89)
Prescribed by ANSI Std. Z39-18
298-102